NASA/TM–2020-220563

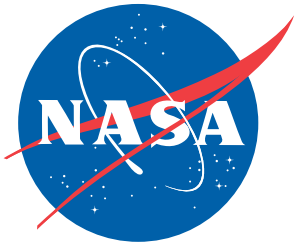

SAGE III ISS Contamination Monitoring Package: Observations in Orbit

Tyler T. Dawson
Science Systems and Applications, Inc., Hampton, Virginia

Charles A. Hill and Amy F. Rowell
Langley Research Center, Hampton, Virginia

Kevin R. Leavor
Science Systems and Applications, Inc., Hampton, Virginia

Sophia Hawley
Langley Research Center, Hampton, Virginia

February 2020

NASA STI Program . . . in Profile

Since its founding, NASA has been dedicated to the advancement of aeronautics and space science. The NASA scientific and technical information (STI) program plays a key part in helping NASA maintain this important role.

The NASA STI program operates under the auspices of the Agency Chief Information Officer. It collects, organizes, provides for archiving, and disseminates NASA's STI. The NASA STI program provides access to the NTRS Registered and its public interface, the NASA Technical Reports Server, thus providing one of the largest collections of aeronautical and space science STI in the world. Results are published in both non-NASA channels and by NASA in the NASA STI Report Series, which includes the following report types:

- TECHNICAL PUBLICATION. Reports of completed research or a major significant phase of research that present the results of NASA Programs and include extensive data or theoretical analysis. Includes compilations of significant scientific and technical data and information deemed to be of continuing reference value. NASA counter-part of peer-reviewed formal professional papers but has less stringent limitations on manuscript length and extent of graphic presentations.

- TECHNICAL MEMORANDUM. Scientific and technical findings that are preliminary or of specialized interest, e.g., quick release reports, working papers, and bibliographies that contain minimal annotation. Does not contain extensive analysis.

- CONTRACTOR REPORT. Scientific and technical findings by NASA-sponsored contractors and grantees.

- CONFERENCE PUBLICATION. Collected papers from scientific and technical conferences, symposia, seminars, or other meetings sponsored or co-sponsored by NASA.

- SPECIAL PUBLICATION. Scientific, technical, or historical information from NASA programs, projects, and missions, often concerned with subjects having substantial public interest.

- TECHNICAL TRANSLATION. English-language translations of foreign scientific and technical material pertinent to NASA's mission.

Specialized services also include organizing and publishing research results, distributing specialized research announcements and feeds, providing information desk and personal search support, and enabling data exchange services.

For more information about the NASA STI program, see the following:

- Access the NASA STI program home page at *http://www.sti.nasa.gov*

- E-mail your question to help@sti.nasa.gov

- Phone the NASA STI Information Desk at 757-864-9658

- Write to:
  NASA STI Information Desk
  Mail Stop 148
  NASA Langley Research Center
  Hampton, VA 23681-2199

NASA/TM–2020-220563

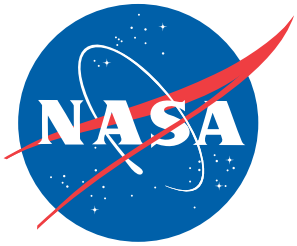

SAGE III ISS Contamination Monitoring Package: Observations in Orbit

Tyler T. Dawson
Science Systems and Applications, Inc., Hampton, Virginia

Charles A. Hill and Amy F. Rowell
Langley Research Center, Hampton, Virginia

Kevin R. Leavor
Science Systems and Applications, Inc., Hampton, Virginia

Sophia Hawley
Langley Research Center, Hampton, Virginia

National Aeronautics and
Space Administration

Langley Research Center
Hampton, Virginia 23681-2199

February 2020

Available from:

NASA STI Program / Mail Stop 148
NASA Langley Research Center
Hampton, VA 23681-2199
Fax: 757-864-6500

Executive Summary

The Stratospheric Aerosol and Gas Experiment III (SAGE III) telescope and instrument assembly employ the methods of solar occultation and lunar occultation to retrieve near-global vertical profiles of atmospheric ozone, water vapor, nitrogen dioxide, aerosol extinctions, and other gaseous species and atmospheric state parameters. The SAGE III grating spectrometer measures light within the spectral range of 280 nm to 1037 nm at approximately 1 nm resolution, but retrievals in the Ultraviolet (UV) are particularly sensitive to contamination of the optical train. Therefore, a contamination door that contains a quartz optical window can be closed over the telescope aperture during periods of enhanced external contaminant flux. This optically transparent window permits continued science event acquisition at an acceptably diminished signal-to-noise ratio, which is expected to decline with ongoing accretion of contaminant material. To date, this impact has been short-term, and science quality through the window returns to baseline performance after a contamination source is removed and spontaneous desorption removes material from the low-affinity quartz surface. Two Contamination Monitoring Packages (CMPs) consisting of eight Thermoelectric Quartz Crystal Microbalances (TQCMs) from QCM Research provide characterization and redundant monitoring of contaminant deposition from the 2π steradian solid angle on the payload side of the Expedite the Processing of Experiments to the Space Station (ExPRESS) Payload Adapter. CMP data are closely examined by the SAGE III team to determine when the contamination door should remain closed during science events and in what direction the instrument assembly scan head should stow when not acquiring science measurements. Additionally, should the CMPs indicate an unacceptable accretion rate, the flight computer will close the contamination door as part of the automatic fault detection system. Along with spectrometer measurements of the quartz window's transmission, the payload CMPs enable auditing of the mission contamination budget. The process of Thermogravimetric Analysis (TGA) can be used to help identify chemical constituents accreted on the CMP sensors. To be presented here along with an explanation of the CMP systems are the first two and a half years of observations of the contaminant deposition environment around the payload in quiescence and during special events like docking vehicles.

Contents

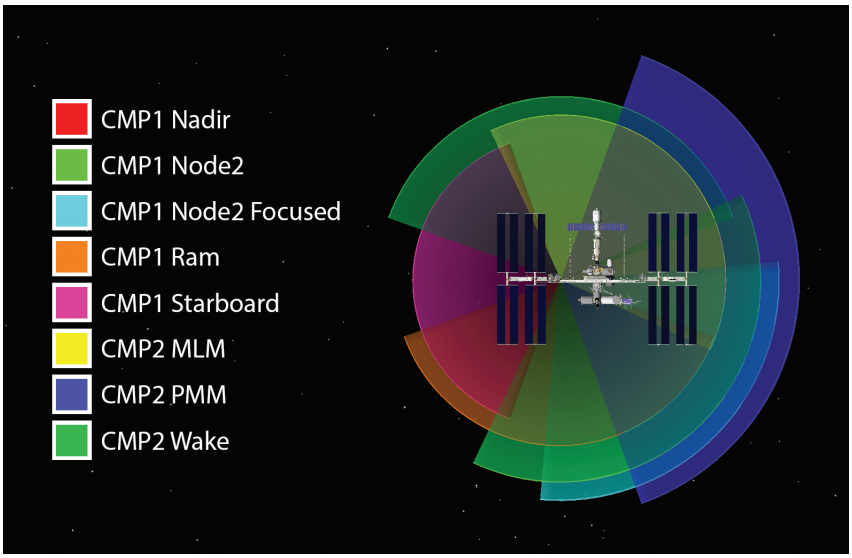

Figure 1: Field of View for All SAGE III CMP Sensors

1 Introduction

1.1 Brief Mission Overview

The Stratospheric Aerosol and Gas Experiment III (SAGE III) was delivered to the International Space Station (ISS) on 23 February 2017 in the unpressurized trunk of the SpaceX Commercial Resupply Services (CRS)-10 Dragon spacecraft. The SAGE III payload was robotically installed on ExPRESS Logistics Carrier-4 (ELC-4) on the nadir side of the S3 Truss and began acquiring atmospheric science measurements on 17 March 2017. The SAGE III telescope and instrument assembly employ the methods of solar occultation and lunar occultation to retrieve near-global vertical profiles of atmospheric ozone, water vapor, nitrogen dioxide, aerosol extinctions, and other gaseous species and atmospheric state parameters. An additional limb scattering mode collects data from the daylit side of the orbit.

The SAGE III grating spectrometer measures light within the spectral range of 280 nm to 1037 nm at approximately 1 nm resolution, but retrievals in the Ultraviolet (UV) are particularly sensitive to contamination of the optical train. Therefore, a contamination door that contains a quartz optical window can be closed over the telescope aperture during periods of enhanced external contaminant flux. This optically transparent window permits continued science event acquisition at an acceptably diminished signal-to-noise ratio, which is expected to decline with ongoing accretion of contaminant material. To date, this impact has been short-term, and science quality through the window returns to baseline performance after a contamination source is removed and spontaneous desorption removes material from the low-affinity quartz surface. Two Contamination Monitoring Packages (CMPs) consisting of eight Thermoelectric Quartz Crystal Microbalances (TQCMs) from manufacturer QCM Research provide characterization and redundant monitoring of contaminant deposition from the 2π steradian solid angle on the payload side

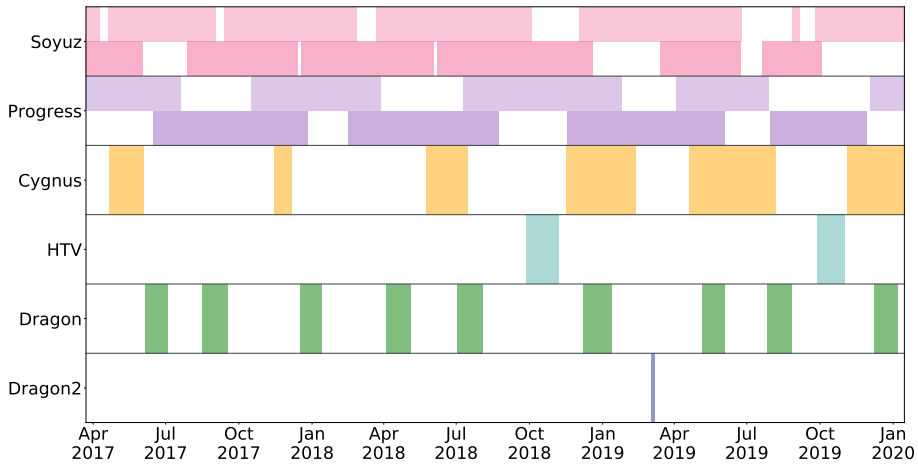

Figure 2: Vehicles That Have Visited the ISS Since SAGE III Deployed

of the Expedite the Processing of Experiments to the Space Station (ExPRESS) Payload Adapter, as seen in Figure 1. CMP data are closely examined by the SAGE III team to determine when the contamination door should remain closed during science events and in what direction the instrument assembly scan head should stow when not acquiring science measurements. Additionally, should the CMPs indicate an unacceptable accretion rate, the flight computer will close the contamination door as part of the automatic fault detection system. Along with spectrometer measurements of the quartz window's transmission, the payload CMPs enable auditing of the mission contamination budget. The process of Thermogravimetric Analysis (TGA) can be used to help identify chemical constituents accreted on the CMP sensors.

1.2 SAGE III Contamination Environment

The ISS contamination environment on ELC-4 was poorly characterized prior to the arrival of SAGE III. The project expected that during mission operations the payload would be exposed to contamination from new ISS modules and new commercial vehicles. Since initial studies and inquiries were unable to specifically identify all contaminants and levels to which SAGE III could come into contact, the CMPs were deployed as a risk mitigation strategy.

It is vital for SAGE III to measure and respond to contaminants to preserve the quality of ozone, aerosol, and other data products. For example mesospheric ozone is retrieved in the UV region of the spectrum and is a primary science product. However, contaminants such as silicates deposited on the instrument scan mirror would absorb in the UV-bands and directly impact the ability to retrieve mesospheric ozone abundances.

Prior to launch it was anticipated that ISS solar panels would be the largest source of contamination. Solar panel contribution to the background contamination over an orbit is coupled to the solar flux term, and exposure to a given QCM is

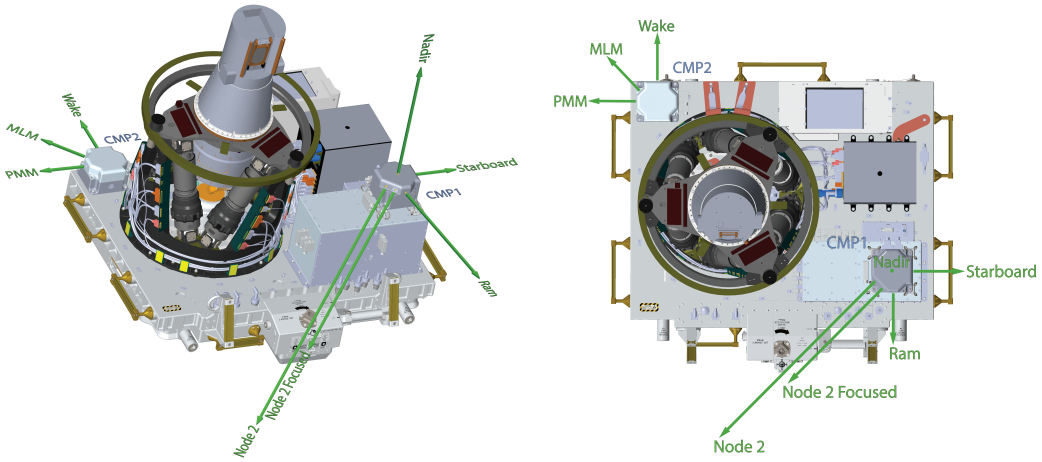

Figure 3: Side and Top Down Views of the SAGE III Payload

related to panel articulation. The solar flux variation over an orbit also induces noise on individual CMP sensors by inducing a thermal gradient across the sensor. This makes characterizing the contamination from solar panels on their own next to impossible.

Visiting vehicles have therefore been the largest source of attributable contamination measured. To mitigate their effects on the instrument, the contamination door is closed when vehicles arrive and depart. However when vehicles not previously observed by the CMPs arrive, the instrument is commanded into SAFE mode for contamination characterization to determine future response.

1.3 ISS Activity

The ISS presents a dynamic environment with a host of activities that potentially impact SAGE III including visiting vehicles, reboosts, venting, attitude maneuvers, and Extravehicular Activities (EVAs).

The CMPs have direct and partial views of many docking ports as indicated in Table 1. Visiting vehicles are the most prominent contamination sources. During SAGE III's time on orbit the following vehicles have visited the ISS: Russian Soyuz and Progress, SpaceX Dragon (CRS) and Dragon2, Japanese H-II Transfer Vehicle (HTV), and Northrup Grumman's Cygnus capsule. The timeline of these vehicle visits can be seen in Figure 2. Detailed analyses for each of the visiting vehicles can be found in Section 3.4.

2 SAGE III/ISS CMPs

2.1 Contamination Monitoring Packages (CMPs)

SAGE III is equipped with two CMP modules: CMP1 and CMP2. CMP1 is located above the Interface Adapter Module (IAM) on the Starboard RAM corner of the ExPRESS Payload Adapter (ExPA) and CMP2 is located at the opposite

CMP Sensor	Direction of View	Field of View	Typically Observed
CMP1 Sensor 0	Starboard	ELC-4	Solar Arrays
CMP1 Sensor 1	RAM	N2 Zenith and Nadir, possibly N2 Fwd	Dragon, Dragon2, HTV
CMP1 Sensor 2	Node 2 Focused	N2 Zenith and Nadir, possibly N2 Fwd	Dragon, Dragon2, HTV
CMP1 Sensor 3	Node 2 Broad	N1 Nadir, N2 Zenith and Nadir, possibly N2 Fwd	Cygnus, Dragon, Dragon2, HTV
CMP1 Sensor 4	Nadir	MRM1 N2 and N1 Nadir	Vehicles on approach
CMP2 Sensor 0	Wake	DC1, SM Aft, MRM1, MRM2	Progress, Soyuz
CMP2 Sensor 1	PMM	DC1, SM Aft, N2 Fwd, N2 Zenith and Nadir, N1 Nadir, MRM1, MRM2	Cygnus, Dragon, HTV, Progress, Soyuz
CMP2 Sensor 2	MLM	MRM1, MRM2, DC1, SM Aft, slightly N2 Nadir	Cygnus, Progress, Soyuz

Table 1: Summary of Important Information for All CMP Sensors

Port WAKE corner of the ExPA as shown in Figure 3. Some overlap between the sensors is incorporated for the purpose of redundancy should sensor failure occur, as shown in Figure 1. This full coverage is supported by CMP1's five sensors and CMP2's three sensors. Two modules are required because of the layout of the main payload, which leads to viewing obstructions for individual CMP sensors.

To monitor contamination that falls onto the payload and science instrument, the entire half space on the nadir side of the payload pallet is covered by the CMP modules. This is desired because contaminants in LEO are in general anisotropic and subject to rarefied gas conduction, a flow regime in which molecular dynamics are dominated by scatter from and adhesion to solid surfaces, and intermolecular collisions are negligible. This is described as the *Free Molecular Flow* regime of Lafferty [6, p. 81–82]. Contamination can only be measured by TQCMs when the contamination source or surface of last scatter is within the crystal Field of View (FOV) because intermolecular collisions fail to redistribute the contaminants. The full details of each sensor FOV are summarized in Table 1.

The CMPs provide information to the internal IAM Fault Detection, Isolation, and Recovery (FDIR) system, which is vital to protection of the instrument and data quality. The ISS environment is dynamic so knowledge of the various ISS activities allows for contamination correlation with events. These data can be provided to the International Space Station Program (ISSP) and relevant parties to investigate the sources of contamination.

2.2 The Quartz Crystal Microbalance

The eight CMP sensors are Mark 24 Thermoelectric Quartz Crystal Microbalances (MK24 TQCMs). Weighing only 4.5 grams, the Mark 24 is currently one of the smallest of its kind. The MK24 TQCMs are used to produce data about the abundance of contaminants near SAGE III.

A MK24 TQCM includes two circular pieces of proprietary QCM Research "AT Sunwise" cut quartz. As shown in Figure 4, each crystal has a gold electrode on the upper side, with a chromium layer bonding it to the quartz surface, and a smaller gold electrode on the underside similarly bonded. The AT Sunwise cut is used to reduce the change in the fundamental shear mode frequency resulting from the temperature variation caused by changes in solar flux loading on orbit. Each MK24 TQCM sensor also has a single-stage Peltier heat pump, which can be used to cool and heat the sensor assembly as commanded.

Quartz is a highly anisotropic material, the stress-strain behavior being described by a fourth order tensor. Therefore the mechanical resonances of the crystal are strongly dependent on the cut. Because of its piezoelectric nature, deformation of the crystal produces a voltage. If introduced into a resonator circuit, feedback achieves an electrical sine wave at the fundamental crystal mode.

The MK24 TQCM crystals oscillate predominantly in Thickness Shear Mode (TSM), as seen in Figure 5, where the top and bottom faces of the quartz slide opposite of each other. The technique of *acoustical energy trapping* is used to confine mechanical vibrations to the center of the crystal, and allow the rim to be clamped

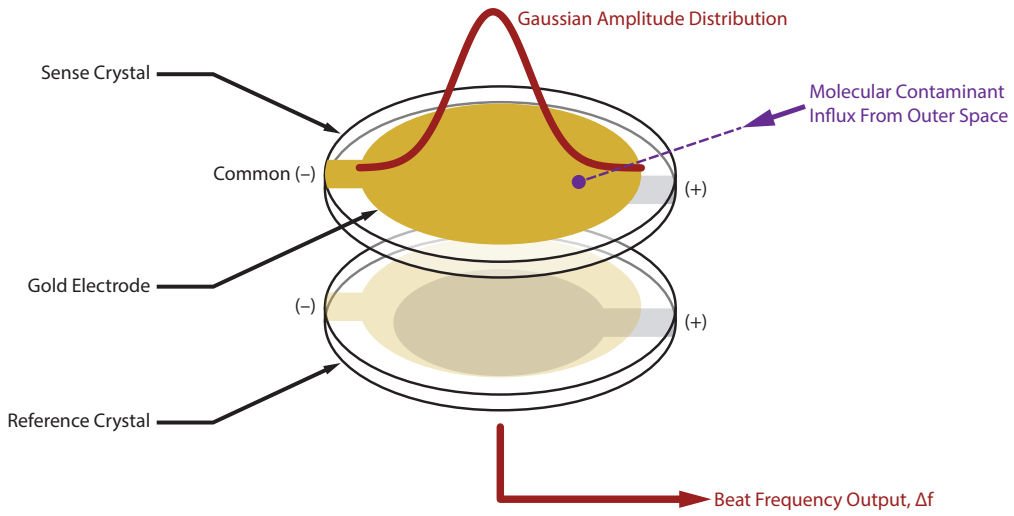

Figure 4: The Thickness Shear Mode vibrations of the crystals are constrained by a Gaussian Amplitude Distribution because the front and back electrodes of each crystal form an acoustic lens, a technique known as *energy trapping*.

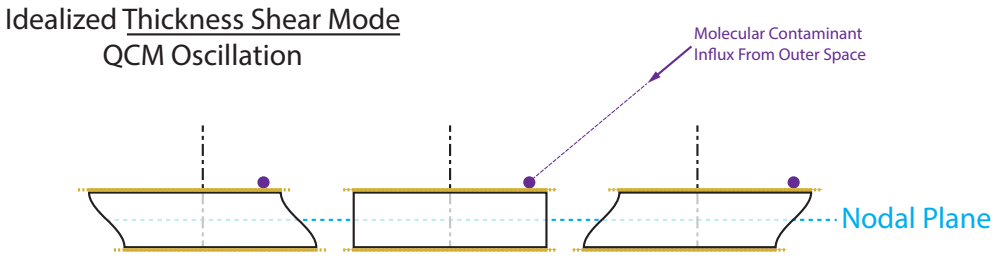

Figure 5: Thickness Shear Mode Depicted on the Sense Crystal in Cross Section. The Reference crystal vibrates similarly.

without adversely affecting resonator Q. The electrode and crystal configuration work to form an acoustical lens that imposes a Gaussian Amplitude Distribution across the crystal, as shown in Figure 4.

The gold electrode on the Sense crystal is exposed to the external environment, allowing particles and molecular contaminants to adsorb to the surface. Lowering the temperature of the crystal using the Peltier element increases its affinity for adsorption. As mass accumulates on the gold electrode, the fundamental frequency of the quartz decreases. However, the TQCM contains a matched quartz crystal oscillator, referred to as the Reference crystal, which serves as a witness that is not exposed to external contamination. The difference between the Sense crystal and the Reference crystal frequencies is known as the *beat frequency*, which is telemetered from each sensor. To determine the amount of mass deposited on the surface area of the sensor over an interval of time, the change in beat frequency is multiplied by the Sauerbrey mass sensitivity constant. For a 15 MHz Sunwise cut crystal with a 2π steradian solid angle field of view, this constant is 1.965 ng/(Hz $\cdot$ cm^2).

For these sensors the relationship between beat frequency and Sauerbrey mass deposition is linear up to 250 kHz. Above 250 kHz, this relationship is nonlinear but oscillation does not cease until 650 kHz. Fundamentally, this relationship will remain linear while in a stable thermodynamic equilibrium, so long as the external excitations are comparable in magnitude to the thermal excitations. With the levels of stress exerted by quartz resonators, soft matter usually obeys linear viscoelasticity. Nonlinearities do occur, but these cases are not as common [4].

2.3 Clausing Conductance Factor

The SAGE III team is currently working on the Clausing conductance derivation for each sensor which will be released with a later revision. Transmission probability, denoted as α, was first introduced by Clausing [3]. If there are N_1 molecules at the entrance plane of a duct then αN_1 will reach the exit plane and $(1-\alpha)N_1$ return to the entrance. If N_0 molecules strike the exit plane from a downstream chamber then αN_0 will reach the entrance. Therefore the net flux of molecules from entrance to exit is $\alpha(N_1 - N_0)$. While this is proportional to the pressure difference, it is actually driven by two independent fluxes as shown in Lafferty [6, p. 86–88]. Thus

the flow dynamics are very different from continuum flow where all molecules that crossed the entrance will leave the exit.

Conductance expressions are formulated with α so that the conductance of a duct C_m is given by the entrance aperture conductance multiplied by the transmission probability. Sensors with different vacuum inlets will acquire different total depositions for the same flux, so Clausing conduction allows you to adjust for flux through an inlet. Thus, the only way to compare two CMP sensors is to compare this corrected external flux.

2.4 Surface Adsorption

Molecular **ad**sorption is a phenomenon of surface chemistry. In contrast, **ab**sorption occurs not at a surface, but within the bulk material. Surfaces are less energetically favored than condensed matter in the bulk because surface molecules exist at a higher energy state—energy must be added to break a solid and form a surface. This leads to two types of energetically favored adsorption.

Physisorption lowers surface energy through van der Waals attraction of atoms or molecules that are only weakly bound to the surface. Physisorption is a reversible bond that breaks more easily at higher temperatures. *Desorption* of contaminants during TQCM temperature ramps implies physisorption and allows for TGA.

When TQCM burn-offs are ineffective, *chemisorption*, an irreversible chemical reaction of a contaminant with the TQCM electrode surface involving strong covalent bonds, is more likely.

Since all atoms and molecules experience long range van der Waals forces, any species physisorbs if the temperature is sufficiently low [5]. The only exception to this occurs when the adsorbate experiences the chemical bond required for it to fall into chemisorption. When this happens, the strength of the chemical bond is governed by two criteria: the degree of filling of the antibonding adsorbate and the strength of the coupling [5].

2.5 Material Selection for Low Earth Orbit (LEO) Environment

SAGE III's placement on the ISS exposes it to the LEO environment. Atomic Oxygen (AO) is present in LEO with a density of 10^9 atoms/cm^3, which corresponds to the density of residual gas in a vacuum of 10^{-7} Torr [9]. The speed of the ISS is roughly 8 km/s. Collisions with highly energetic (5 eV) oxygen atoms are frequent in the orbital RAM direction. Metals such as carbon, aluminum, and silver experience significant mass loss through reaction with AO. Experiments starting with the Long Duration Exposure Facility (LDEF) showed the effects of oxygen erosion. The process to select coating and materials exposed to the LEO environment must consider this interaction [8].

Gold (Au) as an alternative is not as reactive, and chemisorption is unstable. To understand this, the magnitude of the interaction of the bonding level with the metal d band must be considered. This interaction leads to the formation of two levels: one is shifted to lower energies than the bonding state, and the other is positioned slightly higher in energy than the unperturbed metal d band [5].

The lower energy state is bonding with respect to adsorption, while the high energy state is antibonding. As the coupling strength is increased, the orthogonalization energy between the adsorbate and metal d orbitals, which is repulsive, increases. As the d orbitals become more extended, the orthogonalization energy increases. For example, the $5d$ orbitals of Au are more extended than the $3d$ orbitals of copper (Cu). Because of the higher energy cost of orthogonalization between H $1s$ (Hydrogen) and Au $5d$ orbitals, Au is less reactive than Cu [5].

Because gold is less reactive than other metals, it is the ideal choice in LEO for the SAGE III MK24 TQCM electrodes. This material selection avoids ablation of the electrode from the flux of high kinetic temperature AO in LEO.

2.6 Mass and Thickness Calculations

The CMPs report beat frequency f and change in beat frequency Δf for each sensor in telemetry at a rate of 1 Hz. TQCMs are highly precise and accurate for rigid, homogeneous thin films. However, when these assumptions are not met viscoelastic effects emerge, and Sauerbrey calculations are precise but not accurate. This relationship is depicted visually in Figure 6. Therefore, the Sauerbrey mass Δm is a mass equivalent for a rigid, homogeneous thin film. The Sauerbrey mass of a TQCM is directly proportional to Δf as seen in Equation 1. The Sauerbrey thickness d_f as shown in Equation 2 is not to be confused with the geometric thickness; it is the maximum possible thickness.

$$\Delta m = \frac{-A \cdot \sqrt{\rho_q \mu_q}}{2{f_0}^2} \Delta f = -S \cdot \Delta f \tag{1}$$

$$d_f = \frac{-S}{\rho_f} \Delta f \tag{2}$$

A = active surface area $\left(\mathrm{cm}^2\right)$

ρ_q = quartz density $\left(\frac{\mathrm{g}}{\mathrm{cm}^3}\right)$

μ_q = quartz shear modulus $\left(\frac{\mathrm{g}}{\mathrm{cm} \cdot \mathrm{s}^2}\right)$

f_0 = resonant frequency (Hz)

Δf = change in frequency (Hz)

ρ_f = film density $\left(\frac{\mathrm{g}}{\mathrm{cm}^3}\right)$

S = Sauerbrey mass sensitivity $\left(\frac{\mathrm{g}}{\mathrm{Hz} \cdot \mathrm{cm}^2}\right)$

2.7 CMP Thermoelectric Coolers

Each MK24 TQCM is equipped with a Peltier heat pump and Platinum Resistance Thermometer (PRT) that can be used to measure and control the temperature of the quartz crystals. The SAGE III operational temperature range for the TQCMs is from -20°C to 90°C. However, there are applications outside of that temperature range as discussed in Section 3.5.

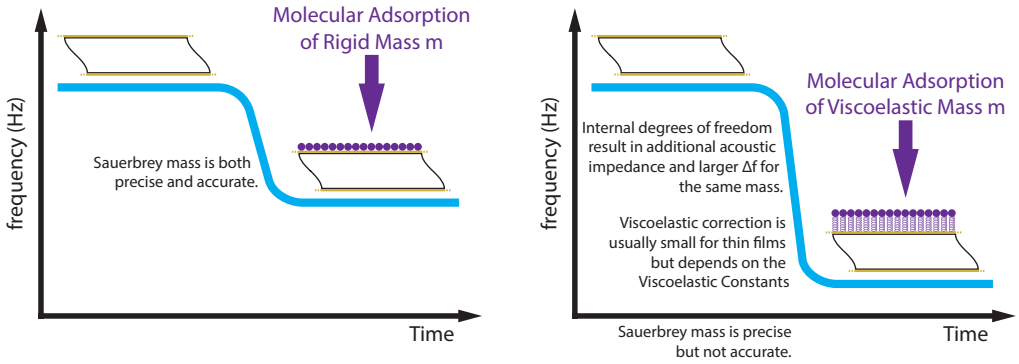

Figure 6: Difference in Adsorption Between Viscoelastic and Rigid Materials of the Same Mass

Per SAGE III requirements, the QCMs must maintain a temperature set-point within $\pm 1.0°C$ and be able to reach a new temperature within 5 minutes. To meet these requirements Proportional-Integral (PI) control loops were implemented electronically in both CMPs so that each TQCM has a separate thermal controller. The combined Peltier heat pump driven by a process control loop is known as a Thermoelectric Cooler (TEC). See Appendix A.1 for detailed equations on how the PI constraints were derived.

In addition to temperature control the TECs are used to run controlled burn offs of contaminants from the TQCMs. Since the crystals become non-linear in response to mass deposition above 250 kHz, and unusable once their beat frequency reaches 650 kHz, both automatic and manual burn-offs are conducted to remove contaminants from the electrodes.

2.8 Telemetry Monitoring

The IAM is continuously monitoring CMP telemetry for violations of software configurable limits. The parameters being monitored include Δf, temperature, voltage, and current. The IAM divides the alerts sent into two categories: warning and critical. When an alert is triggered for one of the monitored telemetry parameters, the payload is able to respond through the FDIR system.

For example, as per Version 21 of the FDIR Document, a warning contamination alert occurs when Δf exceeds 7 Hz/s. This would cause the instrument contamination door to close protecting sensitive optics. A critical contamination alert occurs when Δf exceeds 17 Hz/s, and this causes the payload to command itself into SAFE mode. If the TQCM temperature for any sensor violates the critical upper limit, the payload will stop driving the temperature and return the sensor to ambient. These FDIR responses ensure the safety of the instrument and are necessary to the CMP's role as a FDIR device.

2.9 Electrical Behavior of the QCM: the BvD Model

Contamination is not the only factor that affects the frequency of a TQCM. Various thermal, electrical, and mechanical properties of TQCMs impact stability and precision. The BvD model of a crystal oscillator, as shown in Figure 7, presents the electrically equivalent system of a single TQCM: an LCR branch in parallel with a capacitor. The topology of this equivalent circuit aids in understanding the TQCM sensor's behavior.

The LCR branch represents the mechanical resonances and load of the quartz and is known as the *motional branch*. At series resonance through the motional branch at the crystal's fundamental frequency, the reactances from L and C_1 cancel leaving only real resistance R. Hence, R represents the *motional resistance* or mechanical loading in the quartz that produces acoustic dissipative losses.

The *motional capacitance* C_1 is inversely proportional to the elastic stiffness of the quartz and will vary with cut and temperature. Hence the resonant frequency of the motional branch is temperature-dependent. QCM Research employed a proprietary AT Sunwise cut to minimize the dependence of the elastic stiffness on temperature, but the effect is still observable on orbit in the presence of changing solar flux. The quartz Sense and Reference disks of Figure 4 are clamped around their perimeters to the TQCM housing, and the temperature of the TQCM housing is held constant using a TEC. Were the crystal bulk held at the same temperature as its perimeter, then C_1 would remain stable. However, gold is a poor mirror at solar wavelengths in comparison with, for example, aluminum, and heats as it absorbs sunlight. The rate of heating changes with the angle of the electrode to the incoming sunlight. This heating induces a thermal gradient on the surface of the Sense crystal such that the center of the crystal is at a higher temperature than the perimeter and housing. Differences in the thermal emissivity of the quartz and electrode causes the two materials to cool differently in shade, further augmenting the solar flux-induced noise. These effects result in a varying temperature difference between the contamination sensitive area of the Sense crystal and the Reference crystal. As described in Section 2.5, the LEO environment necessitated the selection of gold for the electrode material, but this selection increased the drift of the series

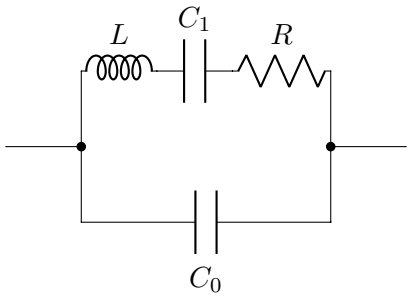

Figure 7: Butterworth-van Dyke Lumped Equivalent Circuit Model of a QCM Crystal

Module	Voltage	Maximum Frequency	Number of Rollovers
CMP1	5 $V_{p\text{-}p}$	320 kHz	4
	7 $V_{p\text{-}p}$	385 kHz	5
CMP2	5 $V_{p\text{-}p}$	300 kHz	4
	7 $V_{p\text{-}p}$	320 kHz	4

Table 2: High Frequency Rollover Test

resonant frequency of the motional branch of the Sense crystal with respect to the Reference crystal with variable solar flux loading. Section 3.6 provides mitigation strategies for this form of noise.

L is the *motional inductance* of the quartz and is proportional to mass, increasing with contaminant deposition on the surface. A Sauerbrey film will increase the motional inductance but leave the stiffness and dissipation the same [4].

The *static branch* contains only the electrical capacitances of the TQCM gold electrodes and to a lesser extent the quartz material itself. Figure 4 clearly suggests that the electrode configuration will exhibit a static, parallel electrical capacitance. The total capacitance of the static branch is represented by C_0.

2.10 CMP Configuration

Both CMPs are powered by the Power Distribution Unit (PDU) integrated into the IAM which supplies 5 V and 15 V of operational power through independent solid-state relays. Both of these power supplies are commanded via serial messages to the PDU. The PDU provides telemetry for CMP voltage and current as well as the 120 V operational heaters.

The CMP modules have the same overall electrical design and are divided into three components: the power board, the main board, and the analog board. A 110-pin stack connector routes power and signals between the boards.

2.11 High Frequency Limits of the CMPs

Analog filters within the CMPs are used to match impedances and condition the beat frequency output signals from the TQCMs to pass to the CMP systems' custom, high-speed Field-Programmable Gate Array (FPGA) frequency counters. When an FPGA frequency counter register reaches 65,535 Hz it will roll over to 1 Hz and indicate a change in beat frequency of 1 Hz/s. Because it is easy to track the number of times a frequency counter rolls over operationally, it is the passband performance of the analog filter that effectively limits the maximum TQCM beat frequency that can be measured by the CMP system and hence the maximum mass of contaminant deposition that can be measured. Laboratory testing of the analog filter design using the project's CMP1 and CMP2 simulators was performed to characterize the high frequency limit. Because the specification of the TQCM component from QCM Research requires the beat frequency output signal to be a sine wave having between 5–7 volts peak-to-peak, both 5 $V_{p\text{-}p}$ and 7 $V_{p\text{-}p}$ signals were tested in an end-to-end fashion through the CMP simulator systems.

CMP Sensor	**Direction of View**	**Total Accretion as of January 2020** $\left[\frac{\mathbf{ng}}{\mathbf{cm^2}}\right]$	**Years Until 250 kHz Threshold**
CMP1 Sensor 0	Starboard	2203.35	369
CMP1 Sensor 1	RAM	1054.22	772
CMP1 Sensor 2	Node 2 Focused	7573.97	107
CMP1 Sensor 3	Node 2 Broad	8776.45	93
CMP1 Sensor 4	Nadir	-117.74	Never
CMP2 Sensor 0	Wake	458.95	1772
CMP2 Sensor 1	PMM	3738.31	218
CMP2 Sensor 2	MLM	1118.24	727

Table 3: Total Mass Accretion as of January 2020 and Time Until the Sensors Reach the 250 Khz Mark **Based on the Current Rate of Accumulation**

Table 2 shows the results of this test. As expected, the higher peak-to-peak voltage signals achieved higher frequencies before being sufficiently attenuated by the analog filters such that the FPGA could no longer count the signals correctly. This behavior confirms that the analog filters are the limiting factors. The number of times the frequency counters rolled over during testing is also shown. The CMP1 simulator registered roughly 30 kHz more than the CMP2 simulator at peak voltage. Overall, the high frequency limits exceeded the linear range of the TQCM sensors (up to 250 kHz) but were lower than the maximum TQCM output (650 kHz).

It is unclear if the upper-frequency limits will be reached because the rate of accumulation is not constant and because new, previously uncharacterized vehicles dock at ISS regularly. However, based on the current rate of accumulation, rollover will not occur during the baseline mission lifetime for either CMP1 or CMP2 as shown in Table 3. Section 3.4 discusses results on this table further.

3 Analysis

The CMPs were initially incorporated into the payload design largely to be used as FDIR devices to protect the SAGE III optical train and to inform mission operations of the contamination environment. However, the CMPs are scientific instruments that can also be used for more in-depth ISS contamination analyses as observed at ELC-4. Properties of some of the contaminants adsorbed on the

CMP sensors can be characterized through TGAs. The TGA technique raises the temperature of the TQCMs at a known rate, and accumulated, physisorbed contaminants will desorb at distinct temperatures during the ramp. Desorption during a temperature ramp causes a relatively sudden drop in the sensor's measured beat frequency. Often, contaminant species can be identified because the unique surface chemistry of each of the species leads to a characteristic desorption temperature. In the following sections the TGA process is described in detail including problems faced, mitigations of these problems, and the current status of the analyses.

3.1 Thermogravimetric Analysis

As mass accumulates on a TQCM it forms a thin film. This causes the effective acoustic thickness of the Sense quartz crystal to increase and hence the beat frequency Δf between the Sense and Reference crystals to increase. As discussed previously in Section 2.4, adsorption by a physisorbed contaminant can be reversed by increasing the temperature of the system. The temperature of each QCM is controlled by a TEC and normally set to $-10°\text{C}$, which is below the desorption temperature of molecular contaminants in the local ISS environment. The low QCM temperature increases the affinity of the sensor to these contaminants and reduces spontaneous desorption through the statistical thermodynamics channel. This increases the resident lifetimes of these contaminants on the sensors. Note that the high kinetic temperature of the local atomic oxygen prevents direct atomic oxygen adsorption to the QCM electrode and can prevent long-term physisorption of contaminants on sensors facing the RAM direction in a process known colloquially as "atomic oxygen scrubbing". The QCM temperature can be commanded by the SAGE III team to perform Thermogravimetric Analyses (TGAs). When an operator initiates a TGA sequence the IAM monitors the TEC temperature and commands it to ramp at a known, steady rate. The resulting Δf as a function of temperature is used to identify contaminant desorption.

The temperature of desorption and Sauerbrey mass m_f (Equation 1 on page 11) are used to calculate fundamental material properties such as specific heat capacities and enthalpies of fusion for the desorbed contaminants. Knowledge of these properties and of the likely contamination sources can lead to the characterization of the contaminant species in the ISS environment. As previously stated, only properties of physisorbed materials are subject to TGA because the process of chemisorption is not reversible over TGA temperatures.

The TQCM data are used to calculate the Sauerbrey mass per unit area on the sensor regardless of the physical properties of the deposited contaminant; Sauerbrey mass is the mass of the rigid and homogeneous thin film (assuming no viscoelasticity) that would induce the equivalent change in beat frequency. Provided the film is thin enough to be considered rigid to the TQCM, the area-averaged mass per unit area can be calculated with accuracy. Note that computing the film thickness cannot be performed accurately without knowing the average mass density of the adsorbed material. Some researchers however report a so-called *Sauerbrey thickness* by using an assumed mass density, most often 1 g/cm^3.

Upon deposition of a thin film it is possible for the quartz piezoelectric stiffening

to change. The rigidity assumption and stiffening change cause the QCM-based gravimetry to have excellent precision but ambiguous accuracy even in the vapor phase [4]. However, if the film is not rigid then non-gravimetric analysis can be performed. Figure 6 on page 11 shows how additional acoustic impedance and hence larger Δf occur for the same mass when it is not rigid. This is why the Sauerbrey mass is an upper bound for non-rigid materials. The viscoelastic mass has internal degrees of freedom into which the acoustic energy is distributed resulting in additional acoustic impedance and increased beat frequency unrelated to mass.

3.2 Spontaneous Desorption

When a TGA is performed, the temperature of the crystal is raised with a linear ramp allowing the molecular species to leave the surface at an increasing rate. During a TGA the vast majority of desorption of a given species occurs at or near its peak desorption rate temperature where roughly one monolayer per second desorbs [5]. However, spontaneous desorption of contaminants at any crystal temperature is also possible through processes such as collisions with hot atomic oxygen or radiation or even thermal cleaving of the surface bond by energy partitioning within the layered canonical ensemble, a statistical thermodynamic channel that will occur even in the absence of external collision. With sufficient time, all molecules physisorbed to a sensor will spontaneously desorb after the source of contamination is removed. The presence of spontaneous desorption imposes a time sensitivity such that a TGA should be performed soon after a vehicle docks to accurately characterize the contaminants being emitted. The SAGE III team targets TGA to begin within one orbit of a vehicle docking and then continues to perform TGAs while the vehicle is docked.

3.3 Quartz Crystal Aging

The downward drift in frequency evident in the Nadir sensor, CMP1 Sensor 4, might be attributed to a slow stress relaxation known as *crystal aging* [4]. Minute plastic strain in the quartz crystal will gradually relax stress loading and is the principal cause of crystal aging. Loading from the electrode bonding process or from the difference in coefficients of thermal expansion between metal and crystal are example sources of unrelaxed stress. Despite being relatively concealed from contaminant sources, the Nadir sensor frequency drift can be seen both in Table 3 and in Figure B26 in Appendix B. According to QCM Research's internal testing, MK24 TQCM sensors should see a change of between 5–51 Hz per year. In general this drift can be a result of a variety of factors including: stress relaxation in the resonator's mounting and bonding structure, electrodes, and in the quartz; oscillator circuit aging from load reactance and drive level changes; quartz outgassing; diffusion effects; and both thermal and hard radiation.

3.4 Vehicle Analysis

As described in earlier sections the ISS is host to a plethora of vehicles, and they have proven to be the largest attributable source of contamination witnessed by the

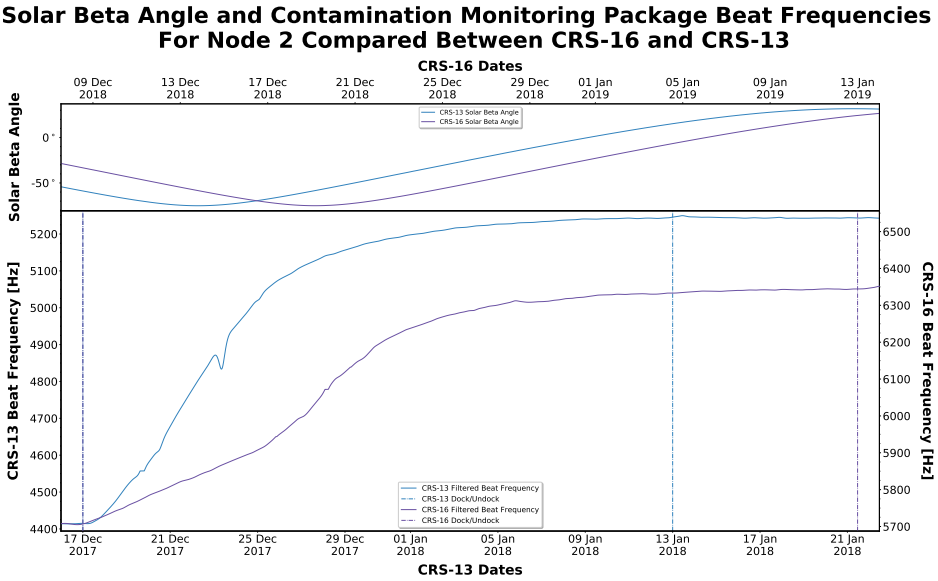

Figure 8: Dragon CRS-13 vs. CRS-16 Visit

CMPs. In the time SAGE III has been on orbit the most impactful contamination events have been the CRS-13 and CRS-16 visits shown in Figure 8, which registered Δf changes on the CMP1 Node 2 sensor of 828.73 Hz and 644.15 Hz, respectively. Both visits occurred during a period of high negative solar beta angle, which causes increased vehicle outgassing towards ELC-4. However, when a TGA was performed on these sensors, the Sauerbrey mass of the contaminant remained unchanged. A burn off was attempted by setting the sensors to 80°C for two weeks, and this likewise yielded no change. These results indicate a contaminant likely chemisorbed to the gold electrodes of the affected sensors.

It has been shown that while silicon is being ablated by AO in LEO, there is an oxidative loss of methyl groups with a gradual conversion to oxides of silicon [1]. Siloxanes are one of the few substances that will chemisorb to a gold surface. Meaning the surface bonding orbitals overcome the antibonding orbitals because of the orbital energy gap, as described in Section 2.5. The siloxanes are converted to silicon dioxide with high temperature rarified AO, and industry has used this effect to successfully coat gold with quartz. This process is more dependent on the high kinetic temperature of LEO AO than photofixation by UV energizing the gold surface. This is one potential source of the accretion on the Node 2 sensors.

The Nadir sensor views most visiting vehicles as they approach the ISS. However, the vehicles are in the sensor FOV for a short duration at a relatively long distance, and therefore the Nadir sensor has not provided insight into the outgassing from these vehicles. While on orbit this sensor has reported a decrease in beat frequency as shown in Table 3. This loss is consistent with crystal aging (Section 3.3).

The MLM sensor, CMP2 Sensor 2, has a FOV that encompasses the Soyuz and Progress docking stations. Historically, these vehicles produce a short period of increased material adsorption on the TQCMs. This material then desorbs within

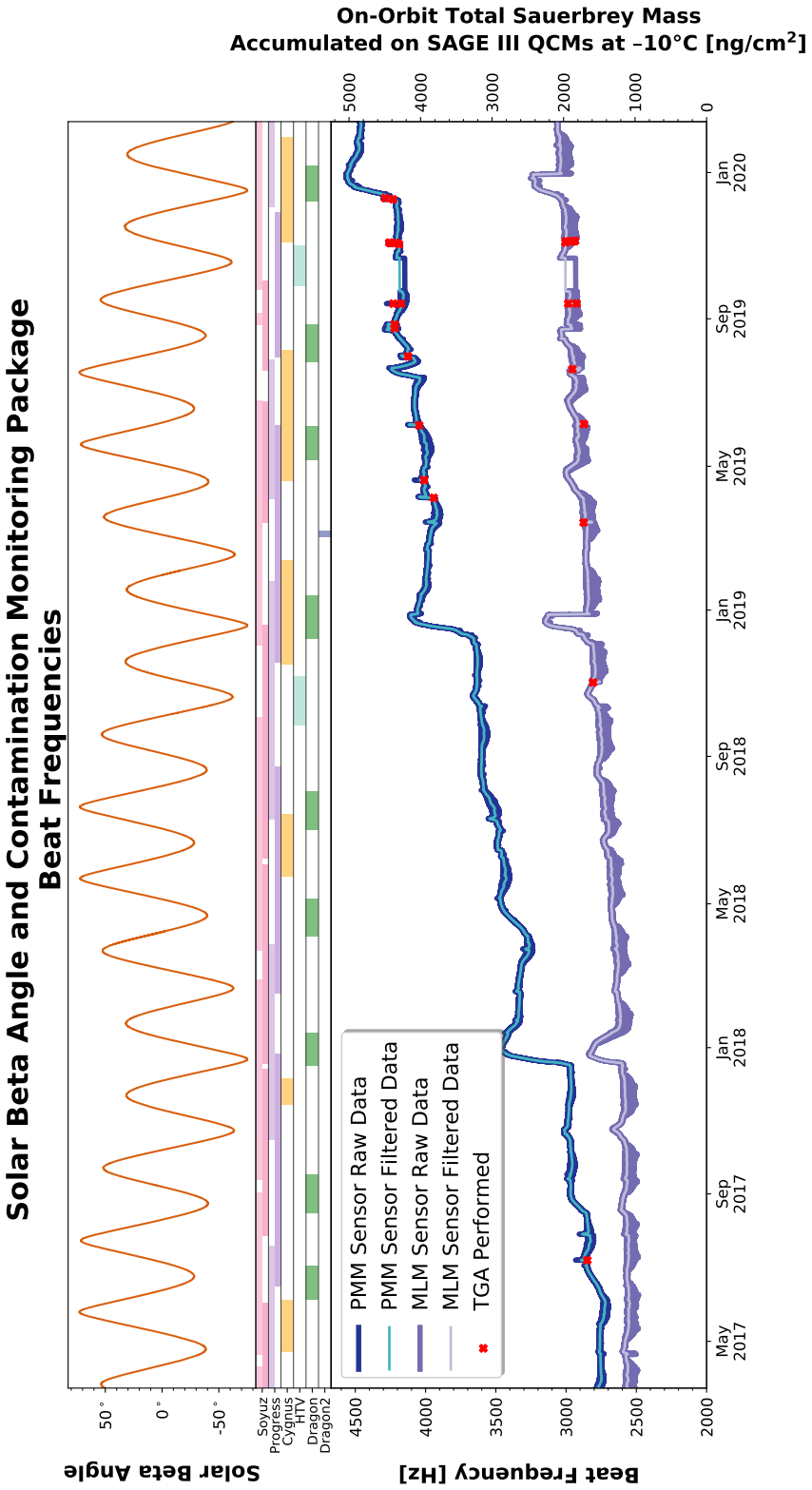

Figure 9: Timeline of Vehicles Visiting the ISS, as Seen by MLM and PMM

a month after material adsorption ends, which can be seen in Figure 9. However the PMM sensor, CMP2 Sensor 1, sees the Soyuz and Progress docking locations and also has a view of the SpaceX Dragon capsule. The material from Soyuz and Progress desorb, but the chemisorbed material does not, (see Figure 9) despite performing multiple TGAs. No meaningful contamination has been observed from HTV or Cygnus.

3.5 Crystal Matching

The dependence of TQCM beat frequency on the temperature of the sensor adds complications to the analysis of TGA results. As the TGA is a temperature driven process, the influence of the sensor temperature on the measured beat frequency must be accounted for and removed from the time series. The SAGE III MK24 TQCMs were delivered from QCM Research with derived 10th-order polynomial temperature correction curves for each sensor. These polynomials were fit using ground calibration data during sensor characterization performed in the course of instrument fabrication and development. The temperature dependence of the measured beat frequency can thus be removed independent of the contamination load on the sensors assuming that the impact of the contamination itself is small or otherwise does not fundamentally alter the sensor and its surface characteristics. Under this scenario, the remaining changes in the measured beat frequency across temperature can be attributed entirely to the adsorption of contaminants to the sensor surface.

The temperature dependence of the measured beat frequency is routinely characterized on-orbit to assess consistency with the ground results. Reassessment of the thermal considerations for the sensors is a crucial part of subsystem trending for their health and aging over time. With respect to sensor aging and the impacts of contamination on each sensor's derived thermal dependence, sensors such as the MLM QCM showing evidence only of physisorption have a re-derived on-orbit temperature correction consistent with the ground-derived curves as shown in Figure 10b. However, sensors such as Node 2 Broad that suggest evidence of chemisorption have drastically different temperature responses on orbit as compared to ground, as shown in Figure 10a.

The SAGE III team has developed operations plans to correct for the impacts of chemisorption and aging over time as in the latter cases above. Each CMP sensor will be commanded to burn off existing contamination, perform TGA ramps both up and down, and produce a beat frequency signal dependent only on the thermal considerations for that sensor. The beat frequency responses from the set of TGA ramps in the up and down directions will be averaged to derive new temperature correction coefficients. The team will periodically revisit these new coefficients to determine if another derivation is necessary following large contamination events.

3.6 Mitigating Solar Flux

Variable lighting and shading of the the ISS from the Sun throughout the orbit induces a time-dependent thermal gradient across the Sense crystals caused by sunlight absorption by the gold electrodes. This is described in more detail in Section 2.9

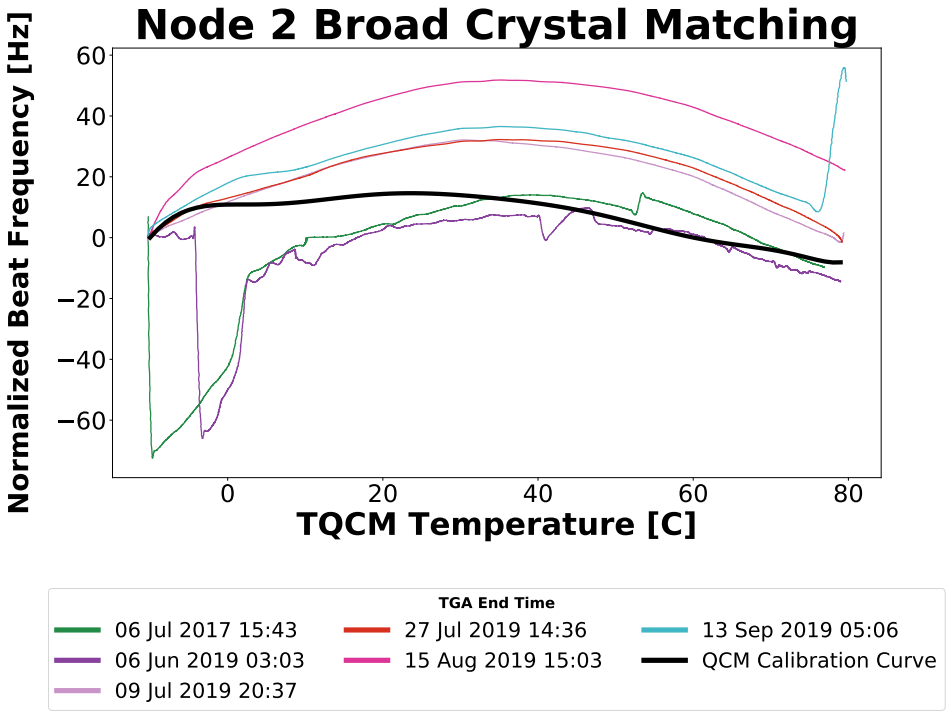

(a) TGAs on Node 2, Which Has Evidence of Chemisorption

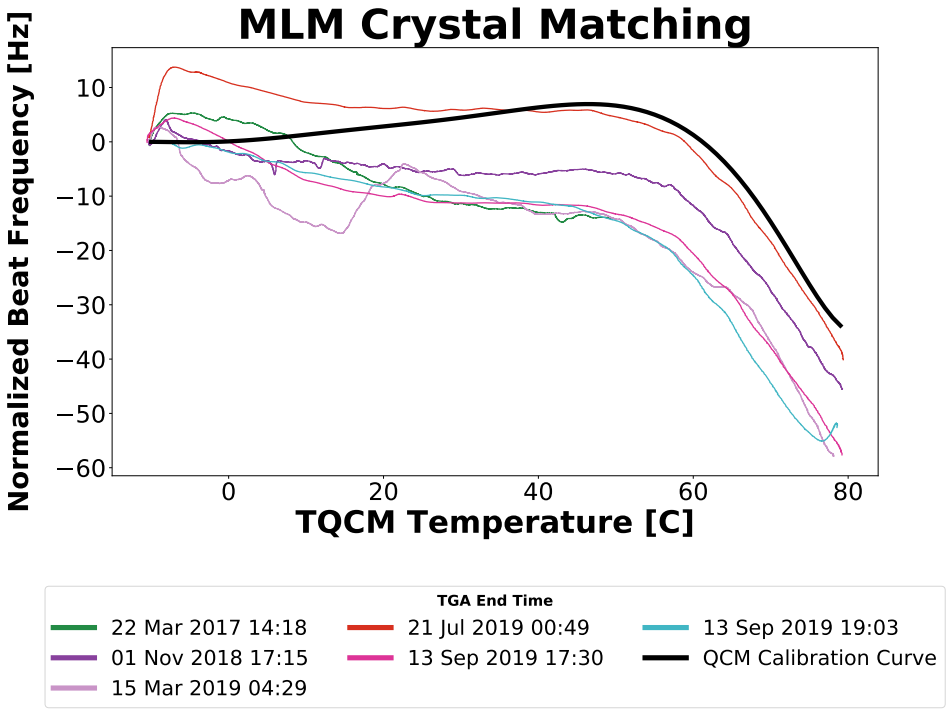

(b) TGAs on MLM, Which Has Evidence of Physisorption

Figure 10: Crystal Matching Comparisons for the Node 2 Broad and MLM Sensors

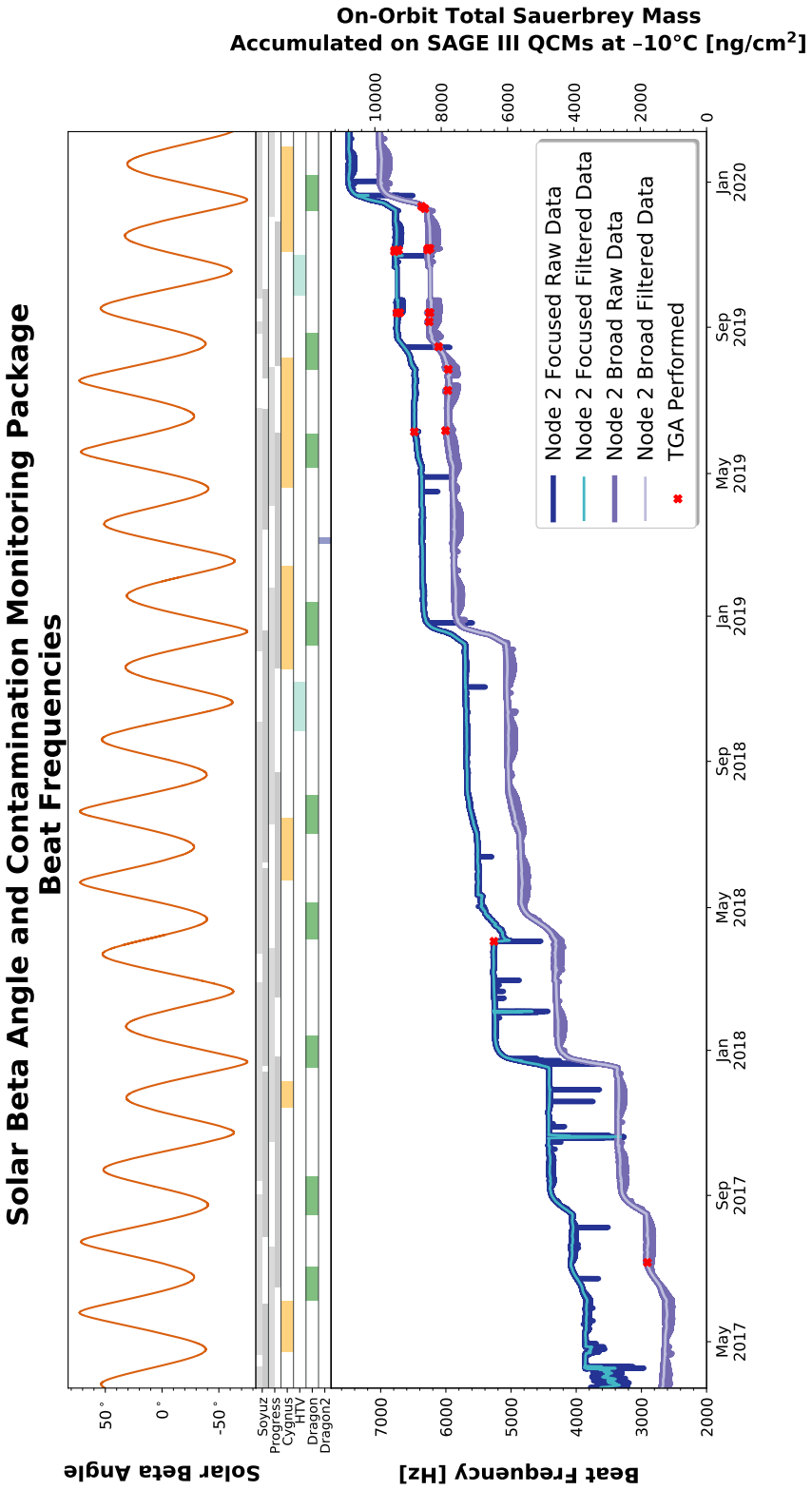

Figure 11: Timeline of Vehicles Visiting the ISS, as Seen by the Node 2 Sensors

as affecting the motional capacitance of Figure 7 on page 13. The magnitude of this thermal dependence is significantly larger than the typical standard deviation of the sensor measurements and contaminant desorption signals. This thermally-induced noise can be seen in the filtered vs unfiltered frequency data shown in Figure 11 and is even more exaggerated during periods of high positive solar beta. Effective use of the beat frequency data for each sensor requires mitigation and removal of the thermally-induced solar signal inherently coupled to the contamination events of interest. This mitigation is even more critical when analyzing TGA events which are of limited duration.

A Butterworth filter has been identified and applied to mitigate the periodic thermal gradient that varies with the ISS orbital period. However, the filter cannot be applied to TGAs because the length of a typical TGA is insufficient to resolve the orbital period, and the magnitude of the noise from the solar flux is much greater than the signal from the desorbed contaminants.

3.6.1 Butterworth Filter

The relationship between the solar beta angle and unfiltered beat frequency can be seen for the Node 2 sensors in Figure 11. At high positive solar beta angle regimes the unfiltered beat frequency is noticeably noisier than at low and negative solar beta angles. This is attributable to different regimes of lighting and shadowing at distinct solar beta angles to the ISS orbit. To discern the desired signal from this solar flux induced noise, a second-order low-pass Butterworth filter was applied to the beat frequency. A Butterworth filter was selected because of its maximally flat passband and linear phase response in comparison with other standard filters. Figure 11 displays both the unfiltered, raw beat frequency and the filtered beat frequency for the Node 2 sensors. Figure 9 is similar for the MLM and PMM sensors. The purpose of the filter is to accurately estimate the sensor signal free from induced solar flux noise.

The cutoff frequency for the Butterworth filter was chosen based on the power spectral density plot shown in Figure 12. The orbital variation in the solar flux term and its accompanying harmonics are highlighted on the upper x-axis, while signals from contamination events can be seen along the y-axis.

The Node 2 Focused, CMP1 Sensor 2, beat frequency is intermittently noisier than that of the other sensors. This behavior was observed rarely during ground testing and later on orbit, and QCM Research was consulted. It was concluded that cross-talk between the sensors induced by faulty grounding is the likely cause. Because Node 2 Broad, CMP1 Sensor 3, has a similar albeit wider FOV, comparisons between the two sensors can be made (correcting for Clausing vacuum conductance through the dissimilar inlets) to ensure that noise is not significantly impacting Node 2 Focused analyses. The enhanced Node 2 Focused noise and the similarity of the two Node 2 uncorrected beat frequencies can be seen in Figure 11.

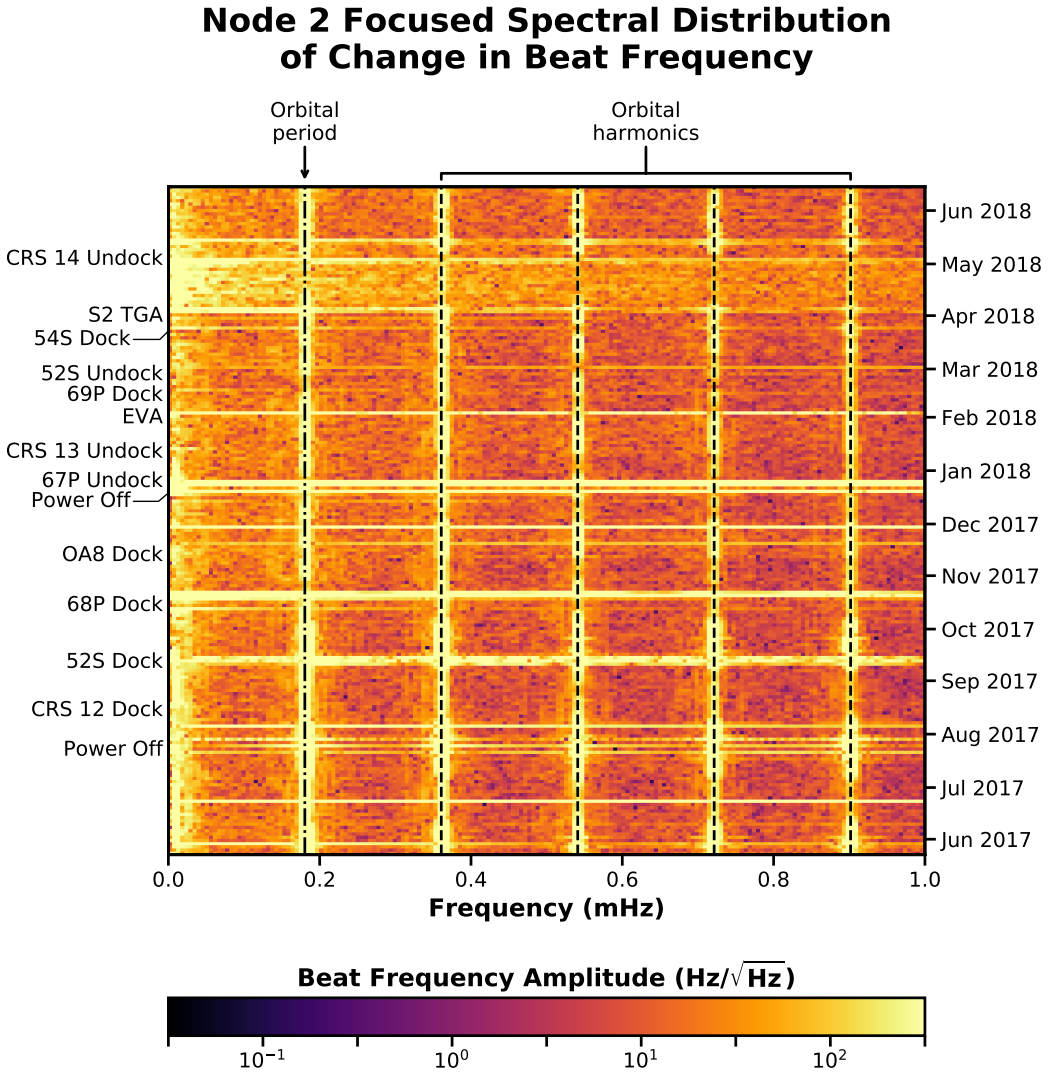

Figure 12: CMP1 Node 2 Focused Spectrogram

Activity	**% Allocation**	**Contamination Levels per Activity** $\left[\frac{\mathbf{ng}}{\mathbf{cm^2}}\right]$	**External Surfaces and Instrument Scan Mirror Accumulated Level** $\left[\frac{\mathbf{ng}}{\mathbf{cm^2}}\right]$
Post-Refurbishment		<750	<750
In-house Transportation	0	750	750
AIT	10	750	1500
Storage and Transportation	0	0	1500
Launch Operations	10	1500	3000
Post-launch and Pre-ops	20	3000	6000
Scientific Operations	60	9000	15000
Total: End of Mission	**100**	**15000**	**15000**

Table 4: External Surface and Scan Mirror Contamination Budget

3.6.2 TGA Duration

The large frequency response caused by solar flux has the potential to complicate the interpretation of TGAs. When a sensor goes into or out of sunlight there is a significant, immediate frequency change. This response is visible in Figure 10a during the TGAs on 06 July 2017 and 06 June 2019 in the range of -10°C to 10°C. These TGAs were performed at a rate of 1°C/min and 0.5°C/min, respectively. To alleviate this sunlight effect, the SAGE III team altered the ramp rate to 3°C/min allowing TGAs to be completed on the dark side of an orbit. The TGAs in Figures 10a and 10b performed on the Node 2 Broad and MLM sensors on the dark side of the orbit are markedly smoother and do not show evidence of a transition from darkness to sunlight or vice versa.

3.7 Contamination Effects on the SAGE III Payload

The two main ways in which contamination can effect SAGE III/ISS are in the optical train and the thermal performance. The optical train is protected with a contamination door that can be deployed anytime a high rate of outgassing is detected. Thermally, small upward trends in subsystem temperatures have been observed which are likely the result of typical aging of silver Teflon surfaces. In general, the maximum rates of temperature increase range from 0.5°C/year to 1.5°C/year. An assessment was performed to determine the projected number of years before a yellow warning limit could be reached for each subsystem (if the current maximum observed rate of temperature increase is assumed to continue). For most subsystems, temperatures are not expected to reach limits for over 10 years. A decreasing temperature trend has been observed across the payload at high positive beta angles.

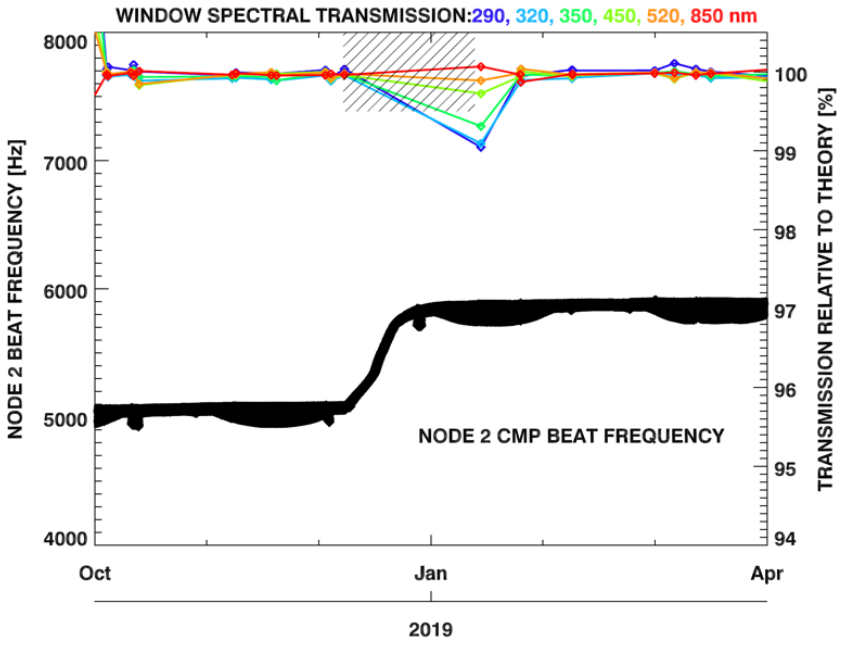

Figure 13: Contamination Window Transmission vs. Wavelength During CRS-16

Investigation into the potential cause of this temperature decrease is ongoing, but decreased temperatures do not present any concern for payload operations since all temperatures are well above minimum operational limits and since all subsystems have operational heaters to ensure safe temperatures are maintained.

3.7.1 Optical Train

As described in previous sections, the SAGE III/ISS instrument is equipped with a contamination door to safeguard sensitive optics and preserve science data quality. During SAGE III/Meteor–3M—the previous iteration of SAGE III that operated from a sun-synchronous orbit aboard the Russian Meteor–3M spacecraft from February 2002 through December 2005—the UV-band was lost within the first six months of the mission because of contamination on the boresight scan mirror. SAGE III is able to acquire science events with the door either opened or closed. When closed to mitigate contamination events, science measurements may be made through a quartz window. Permanent contamination accreted to the quartz window would diminish measurement quality through the window. Analyzing data obtained with the door closed indicates that closure of the contamination door has successfully prevented significant contamination from entering the optical train of the instrument. Figure 13 demonstrates that although transmission through the quartz window is impacted by contaminants while the contamination door is closed, transmission has to date returned to normal over time. This recovery implies that contaminant species are spontaneously desorbing off of the window.

The window has allowed for science acquisition with an acceptable, transiently diminished signal-to-noise ratio. Recall that in Section 3.4 the CRS-16 visit in

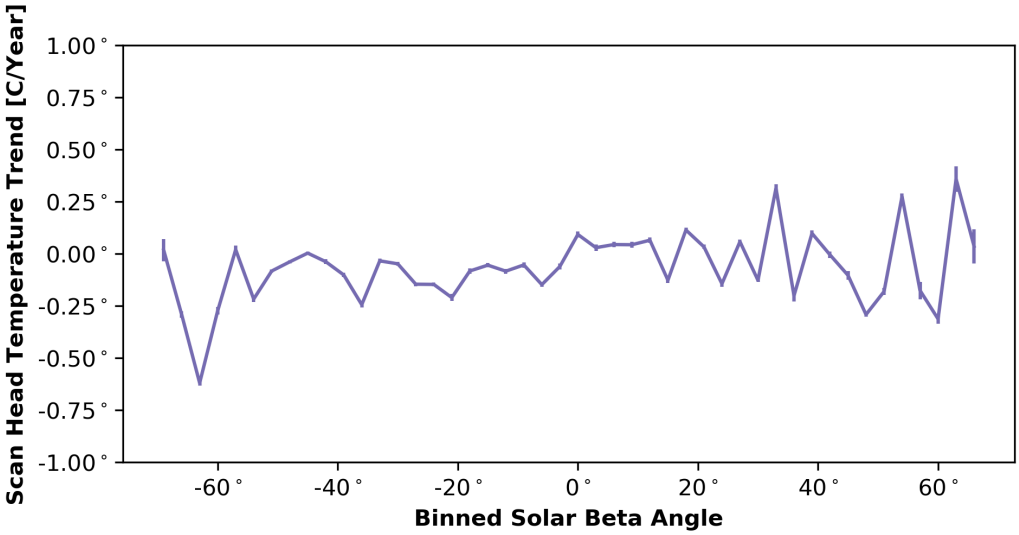

Figure 14: Scan Head Trend vs. Binned Solar Beta Angle

late 2018 corresponded to a significant beat frequency increase for the sensors facing ISS Node 2. The equivalent Sauerbrey deposition is 1265.75 nanograms of contaminants per cm^2 of sensor area. Figure 13 shows the window transmission response during the CRS-16 visit with an approximate 1% decrease in transmission in the lower wavelength channels. The observed maximum transmission dip has been approximately 2% over the mission lifetime so far. After a vehicle departs, the transmission has gradually returned to baseline. Each class of visiting vehicle has been self-consistent and exhibits similar behavior. The contamination door aids in ensuring that the instrument scan mirror remains within the predefined contamination budget of the mission, displayed in Table 4. The values in Table 4 were developed using the Beer-Lambert-Bouguer law [2] and taking into consideration the payload optical and thermal performance requirements.

3.7.2 Thermal Performance

It is impossible to know with certainty if contaminants are desorbing off of other payload surfaces of interest, such as thermal control surfaces, and at what rate. However, the CMPs allow the project team to conservatively monitor overall payload contamination exposure by maintaining sensors at the $-10°C$ high-affinity temperature. Similar to the quartz window, other payload surfaces of interest are likely to not retain a significant portion of the contaminants to which they are exposed. An example of this is shown in Figure 14, which depicts the Scan Head temperature trended over time against solar beta angle.

Total retained deposition above the maximum value listed in Table 4 is expected to noticeably erode the solar absorptance margin of the Silver-Backed Fluorinated Ethylene Propylene Teflon (AgFEP) high-emissivity thermal control surfaces. See Tribble [7, p. 13–17] for in-situ measurements and graphs relating to

the degradation in thermal control surfaces because of solar absorptance. Contamination typically affects the emissivity of a thermal control surface far less than it increases solar absorptance [7]. If molecular contamination is transparent to the radiated wavelength, then the emissivity is largely unchanged. If opaque, then the contamination layer acts as the radiator at the equilibrium temperature of the thermal control surface. Radiator emissivity will be unaffected unless contamination decreases the thermal conductivity significantly. The emissive effects of molecular contamination on low-emissivity surfaces, however, are much more severe. All payload temperatures must be trended over time to gauge these surface effects.

Recall from Section 1.1 that CMP data inform the SAGE III project's decision concerning the azimuthal position to stow the instrument scan head between science events to avoid contamination of the aperture optics. The scan head is currently configured to stow the aperture facing the starboard direction. As shown in Figure 15, starboard is one of cleanest directions and has accumulated very little deposition. The stow direction is periodically reevaluated to ensure the scan head optical aperture is not unnecessarily exposed to contamination. This is an additional precaution to minimize the contamination impact to the science data product.

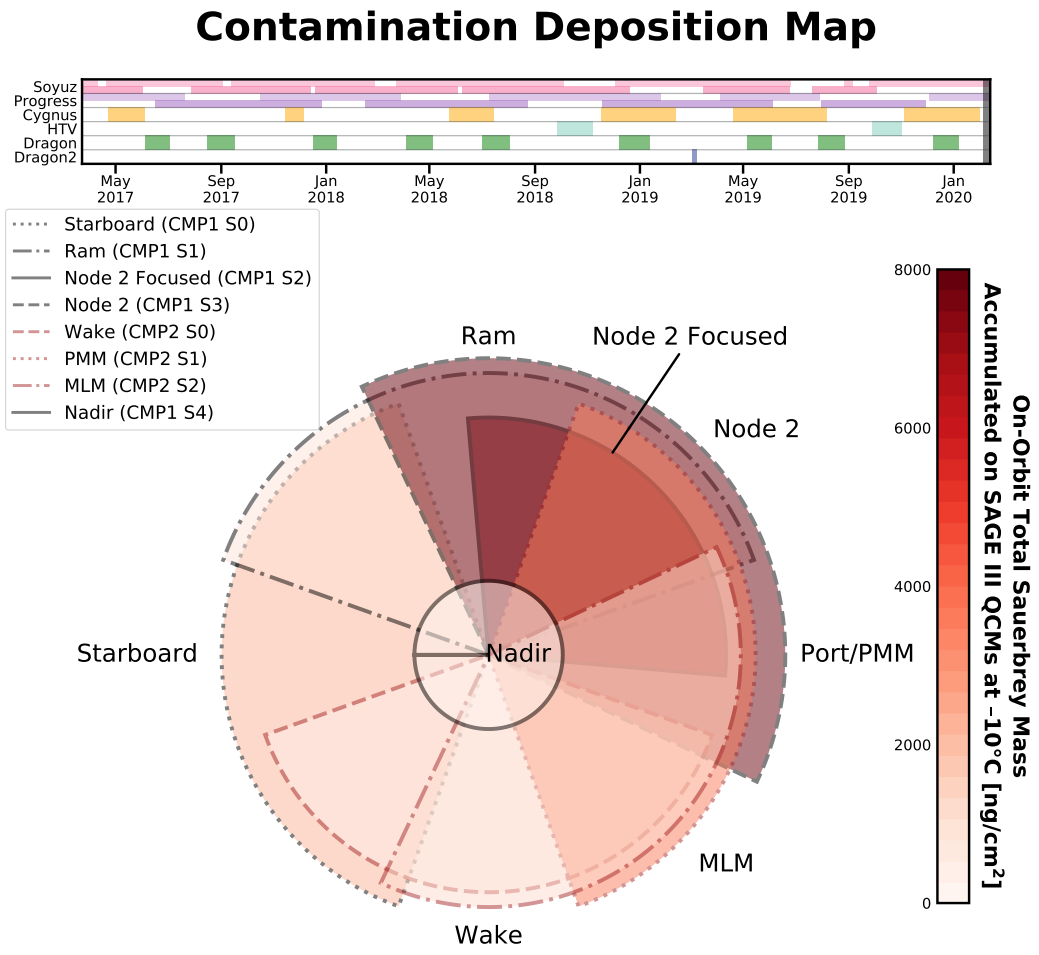

Figure 15: Current Deposition Map of the CMP Sensors

4 Lessons Learned On Orbit

4.1 Inlets Matter

The MK24 TQCM inlet cap is a quality critical part manufactured by QCM Research to a 0.0005 inch tolerance to tightly control gas conductance to the sensor. The sensors in each CMP subsystem were slightly recessed below the chassis during payload development in an attempt to protect them from damage. When it was determined that a CMP sensor was needed to focus on the docking port Node 2, CMP1 Sensor 3 "Node 2 Focused" was effectively further recessed into the housing by the addition of a flanged spacer on the inlet to narrow the half-angle FOV. However, these actions complicate calculation of the Clausing conductance factor and half-angle FOV for each sensor. In a rarefied gas environment the interaction between gas molecules becomes negligible, and therefore the interaction of the gas molecules with the inlet dominates the flow [6]. Because of changes in the SAGE III inlet design while on the ground, the team must re-derive the Clausing conductance factor for all sensors while on orbit for inlet geometries that were less tightly controlled. The apertures formed by the chassis recesses impact the molecular conductances to the sensors significantly.

If strictly necessary to have, modifications to sensor inlets should be considered carefully and be designated quality sensitive with thought given to how the modification will impact the half-angle and conductance factor. If accurately measuring contaminant flux is important, for example, to make comparisons between broad and focused sensors or for science measurements of contamination, future missions are advised to not recess sensors unless inlet dimensional and assembly tolerances are carefully controlled and sufficiently simple that a Clausing conductance factor can be derived using standard vacuum science principles such as comprehensively described by Lafferty [6]. Ideally, controlling the Clausing conductance factor should be a system design requirement.

4.2 Solar Flux Complications

The nature of the environment onboard the ISS causes several difficulties in analyzing CMP data. Solar flux onto the sensor causes a high amplitude periodic signal. This is further complicated by the varying solar-beta-angle-dependent shade from the ISS. As explained in Section 3.6 these problems were mitigated by increasing the temperature ramp rate of TGAs to restrict TGAs to the dark side of the orbit and by implementing a digital Butterworth filter in post processing to extract the underlying signal.

Several tools are being tested to further analyze these data and extract a meaningful desorption signal. The tools include a Savitzky-Golay filter, Principal Component Analysis (PCA) and comparison of ground test data with measurements from orbit.

References

1. Banks, B. A., Karniotis, C. A., Dworak, D., and Soucek, M. (2004). Atomic oxygen durability evaluation of a UV curable ceramer protective coating. Technical Memorandum NASA/TM-2004-213098, National Aeronautics and Space Administration. Prepared for the Seventh International Conference on Protection of Materials and Structures from Space Environment, Toronto, Canada, May 10–13 2004. DOI: 10.1007/1-4020-4319-8_23.

2. Beer, A. (1852). Bestimmung der absorption des rothen lichts in farbigen flüssigkeiten [Determination of the absorption of red light in colored liquids]. *Annalen der Physik*, 162(5):78–88. DOI: 10.1002/andp.18521620505.

3. Clausing, P. (1971). The flow of highly rarefied gases through tubes of arbitrary length. *J. Vac. Sci. Technol.*, 8(5):636–646. Translated from the German [*Ann. Physik* (5)12:961 (1932)]. DOI: 10.1116/1.1316379.

4. Johannsmann, D. (2015). *The Quartz Crystal Microbalance in Soft Matter Research: Fundamentals and Modeling*. Soft and Biological Matter. Springer International, Switzerland. ISBN-13: 978-3319078359.

5. Kolasinski, K. W. (2012). *Surface Science: Foundations of Catalysis and Nanoscience*. John Wiley & Sons, Chichester, West Sussex, UK, 3^{rd} edition. ISBN-13: 978-1119990352.

6. Lafferty, J. M., editor (1998). *Foundations of Vacuum Science and Technology*. John Wiley & Sons, New York, NY. ISBN-13: 978-0471175933.

7. Tribble, A. C. (2000). *Fundamentals of Contamination Control*, volume TT44 of *Tutorial Texts in Optical Engineering*. SPIE Press, Bellingham, Washington. ISBN-13: 978-0819438447.

8. Whitaker, A. F. and Kamenetzky, R. R. (1993). Atomic oxygen erosion considerations for spacecraft materials selection. In *LDEF Materials Results for Spacecraft Applications*, pages 117–123, Huntsville, Alabama. NASA Marshall Space Flight Center. N94-31012 09-12.

9. Zimcik, D. G. and Maag, C. R. (1987). Results of apparent atomic oxygen reactions with spacecraft materials during shuttle flight STS-41G. *J. Spacecraft*, 25(2):162–168. Presented as paper 85-7020 at the AIAA Shuttle Environment and Operations II Conference, Houston, TX, Nov. 13–15 1985, DOI: 10.2514/3.25965.

Appendix A

PID Thermal Controller

A.1 Description of Variables

The PI thermal controller maintains each TQCM temperature set-point to within $\pm 1^{\circ}$C. To reach a new temperature within five minutes a PI control loop was implemented. Each TQCM has a separate thermal controller.

The transfer function defined by Figure A16, is for a Proportional-Integral-Differential (PID) controller in the discrete time domain. The implemented PI controller is the equivalent of a PID controller with the derivative term D set to zero. The use of a PI controller provides a smoother yet slower response than a PID controller and minimizes overshoot. The PI controller is sufficient for this TQCM temperature loop.

The combined transfer function $G_i(\mathrm{z})$, shown in Figure A17 models the transfer functions $G_2(\mathrm{z})$, $G_3(\mathrm{z})$, and $G_4(\mathrm{z})$.

$G_t(\mathrm{z})$ is the thermal response of the TQCM sensors and is the combination of $G_5(\mathrm{z})$, $G_6(\mathrm{z})$, and $G_7(\mathrm{z})$. This thermally responds to current from $G_i(\mathrm{z})$, so the PID controller's K_g term is the inverse of $G_i(\mathrm{z})$ gain multiplied by $G_t(\mathrm{z})$ gain, shown in Figure A18.

K_g is the "Fudge Factor" to make the total open loop transfer function a unity gain.

K_p is the proportional gain term of the PID loop.

K_i is the integral gain term of the PID loop.

b_0 and b_1 are configurable parameters defined in Figure A19. b_0 and b_1 are set for each CMP module independently. The values used on orbit for both modules are $b_0 = 2824$ and $b_1 = 62758$. These values can be rederived on the ground and updated on flight as needed.

The total open loop transfer function is defined by Figure A20 and the closed loop transfer function is defined by Figure A21.

A.2 Equations and Functions

$$G_1(z) = \frac{M(z)}{E(z)} = K_g \left[K_p + \frac{K_i T}{2} \left(\frac{z+1}{z-1} \right) \right] \tag{A3}$$

$$G_1(z) = \frac{\left(K_g K_p + \frac{K_g K_i T}{2} \right) + \left(-K_g K_p + \frac{K_g K_i T}{2} \right) z^{-1}}{(1 - z^{-1})} \tag{A4}$$

Figure A16: PID Transfer Function

$$G_i(z) = \frac{M_4(z)}{M(z)} = K_a = 1.8 \tag{A5}$$

Figure A17: PID Effort to Current Transfer Function

$$K_g = \frac{8}{K_a K_b} \tag{A6}$$

Figure A18: "Fudge Factor" Unity Gain

$$b_0 = K_g - K_p + \frac{K_g K_i T}{2} \tag{A7}$$

$$b_1 = -K_g K_p + \frac{K_g K_i T}{2} \tag{A8}$$

$$a_1 = -1 \tag{A9}$$

$$y[n] = b_0 x[n] + b_1 x[n-1] - a_1 y[n-1] \tag{A10}$$

Figure A19: PID Difference Equation

$$G(z) = G_1(z) G_i(z) G_t(z) \tag{A11}$$

Figure A20: Thermal Controller Open Loop Transfer Function

$$H(z) = \frac{Y(z)}{X(z)} = \frac{G(z)}{1 + G(z)} \tag{A12}$$

Figure A21: Thermal Controller Closed Loop Transfer Function

Appendix B

Timeline Graphs

For the following graphs the plots are ordered as such: the top plot denotes the solar beta angle of the ISS orbit, the middle plot is a vehicle arrival/departure timeline, and the bottom plot is the sensor beat frequency and Sauerbrey mass density (relative to a beat frequency of 0 Hz) as of the publication of this document. Grayed out vehicles in the timeline indicate that the respective vehicle is not in the sensor FOV.

In reality an attempt was made to match the Sense and Reference crystals such that clean sensors (meaning 0 ng/cm^2 sensor accretion) will exhibit approximately a 2 kHz beat frequency. Hence the Sauerbrey mass densities in the following plots must be interpreted *relatively* between two points in time to ascertain actual accretion. That is, if the mass deposition per sensor surface area is, say, shown as 5200 ng/cm^2 at the start of the time line and 5400 ng/cm^2 at the end of the time line, then the full time line shows a Sauerbrey mass deposition of 200 ng/cm^2, the starting value of 5200 ng/cm^2 not representing a real mass.

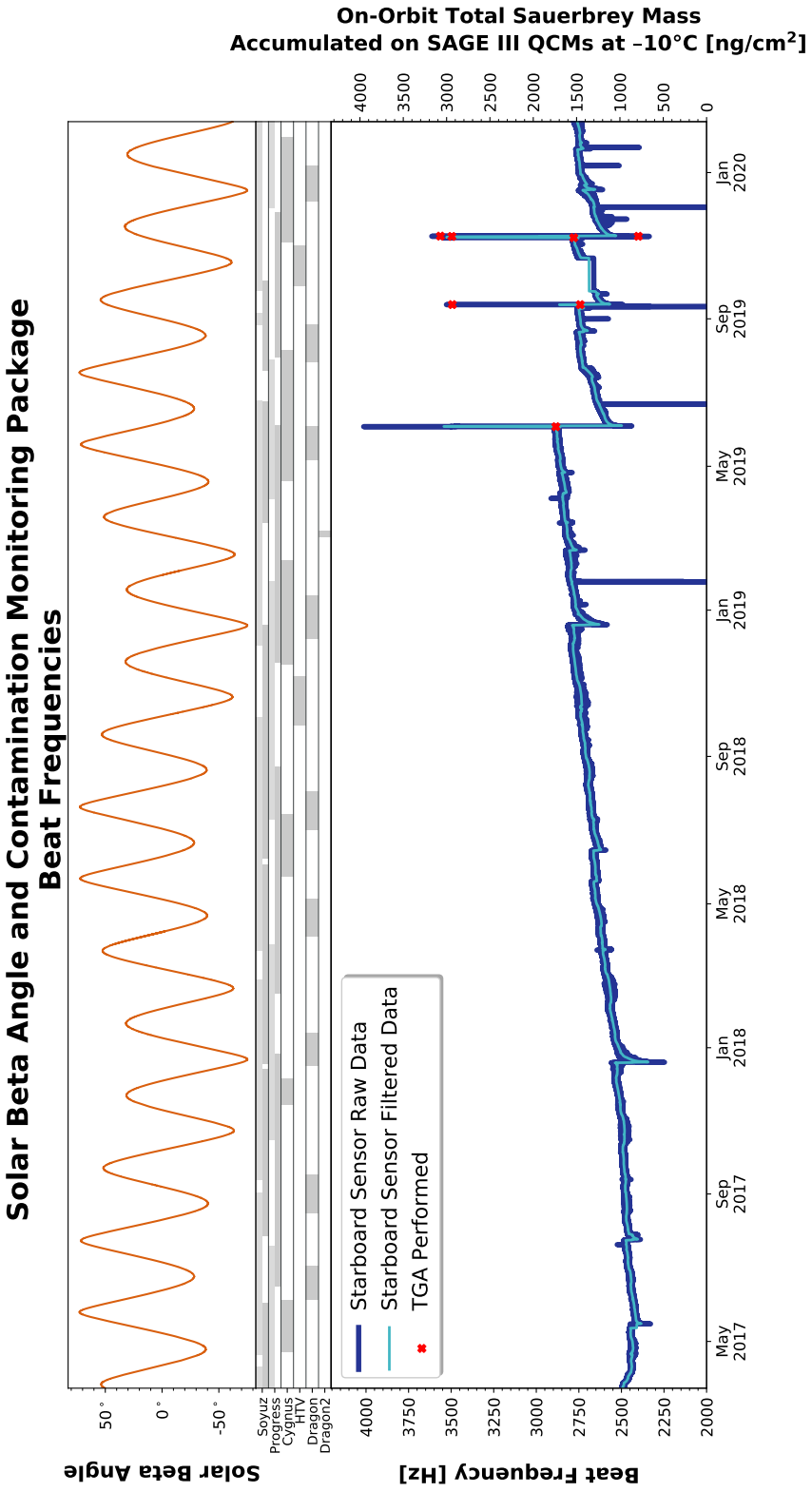

Figure B22: Timeline of Vehicles Visiting the ISS, as Seen by the Starboard Sensor

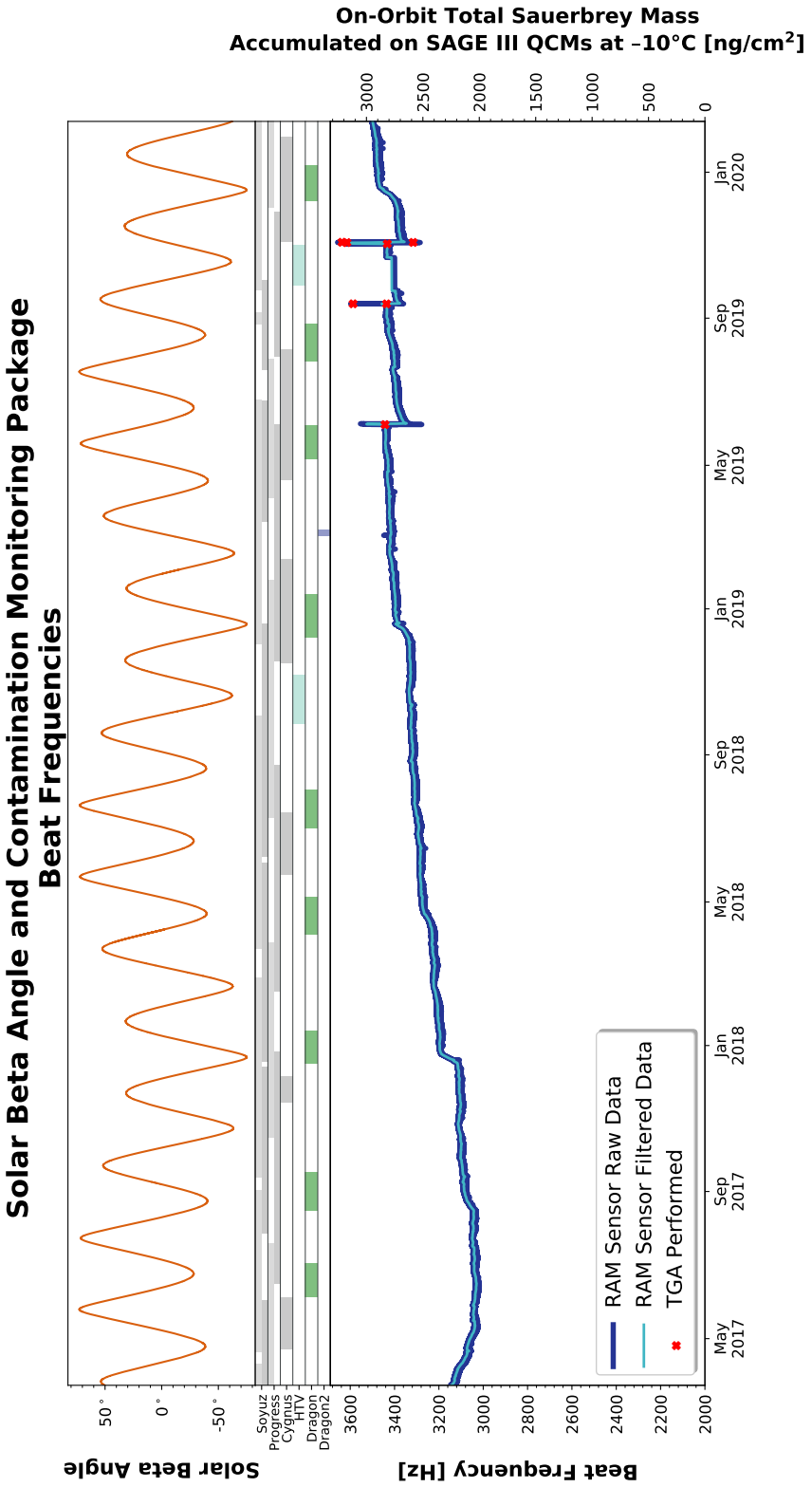

Figure B23: Timeline of Vehicles Visiting the ISS, as Seen by the RAM Sensor

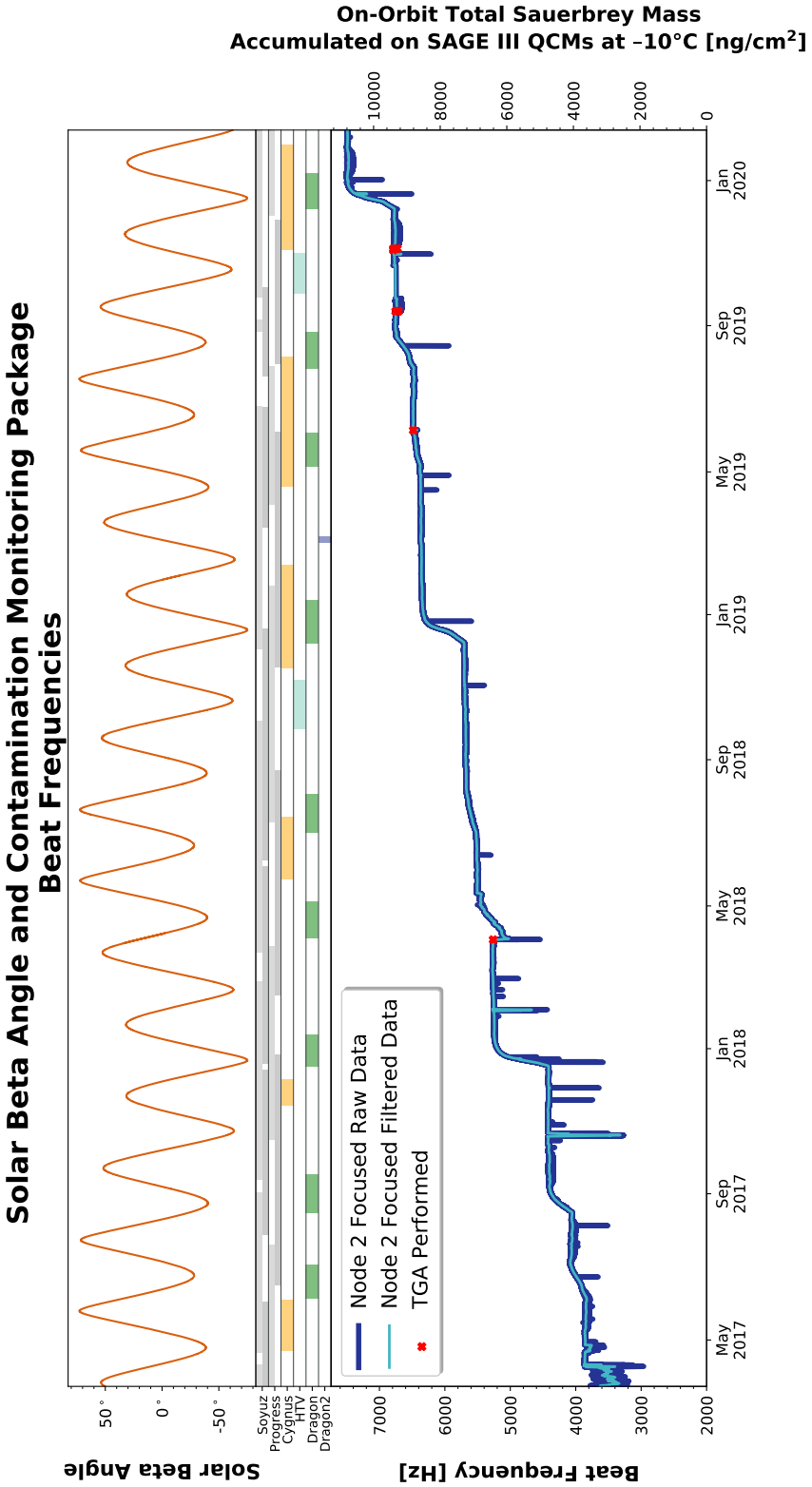

Figure B24: Timeline of Vehicles Visiting the ISS, as Seen by the Node 2 Focused Sensor

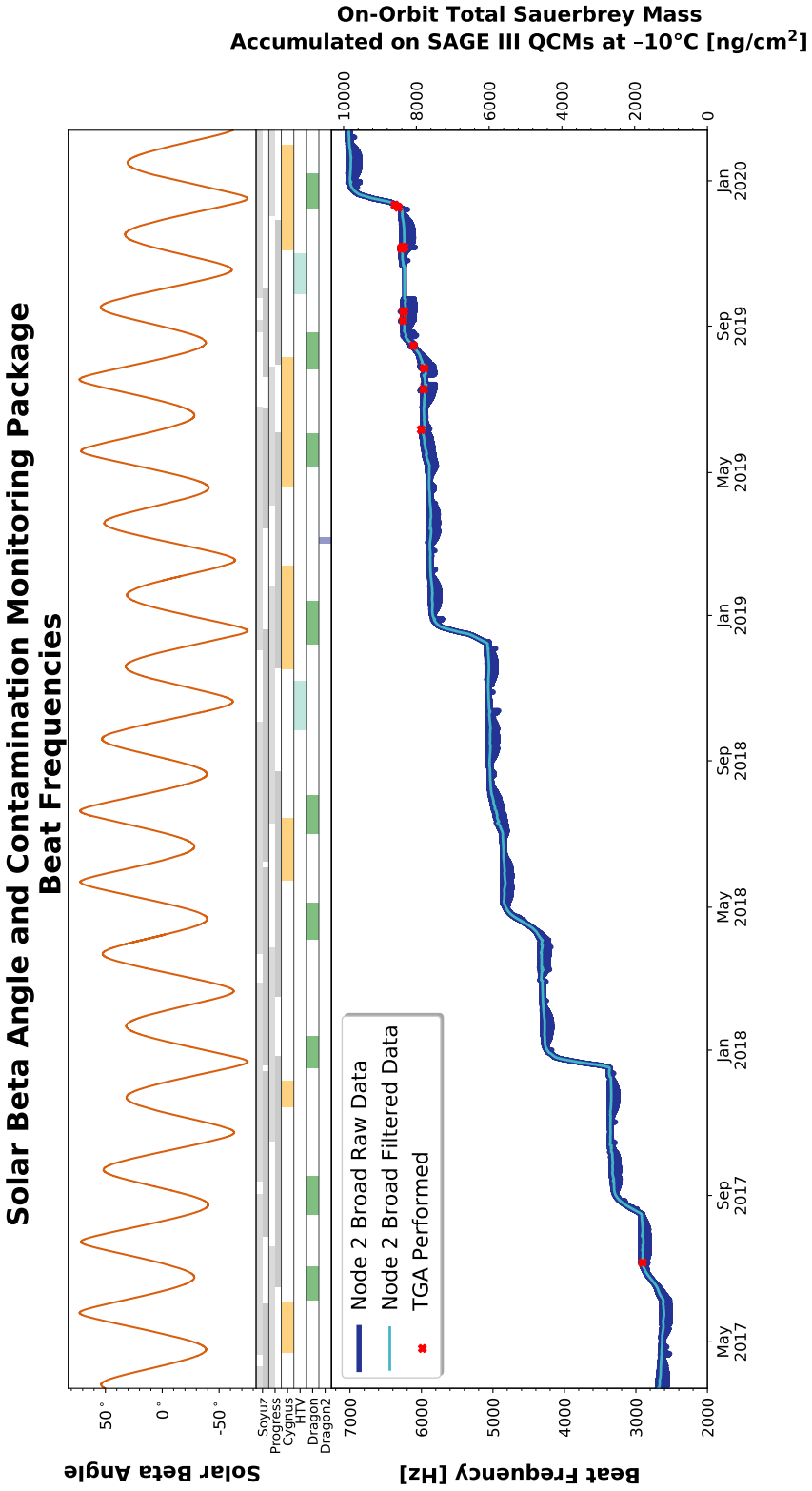

Figure B25: Timeline of Vehicles Visiting the ISS, as Seen by the Node 2 Broad Sensor

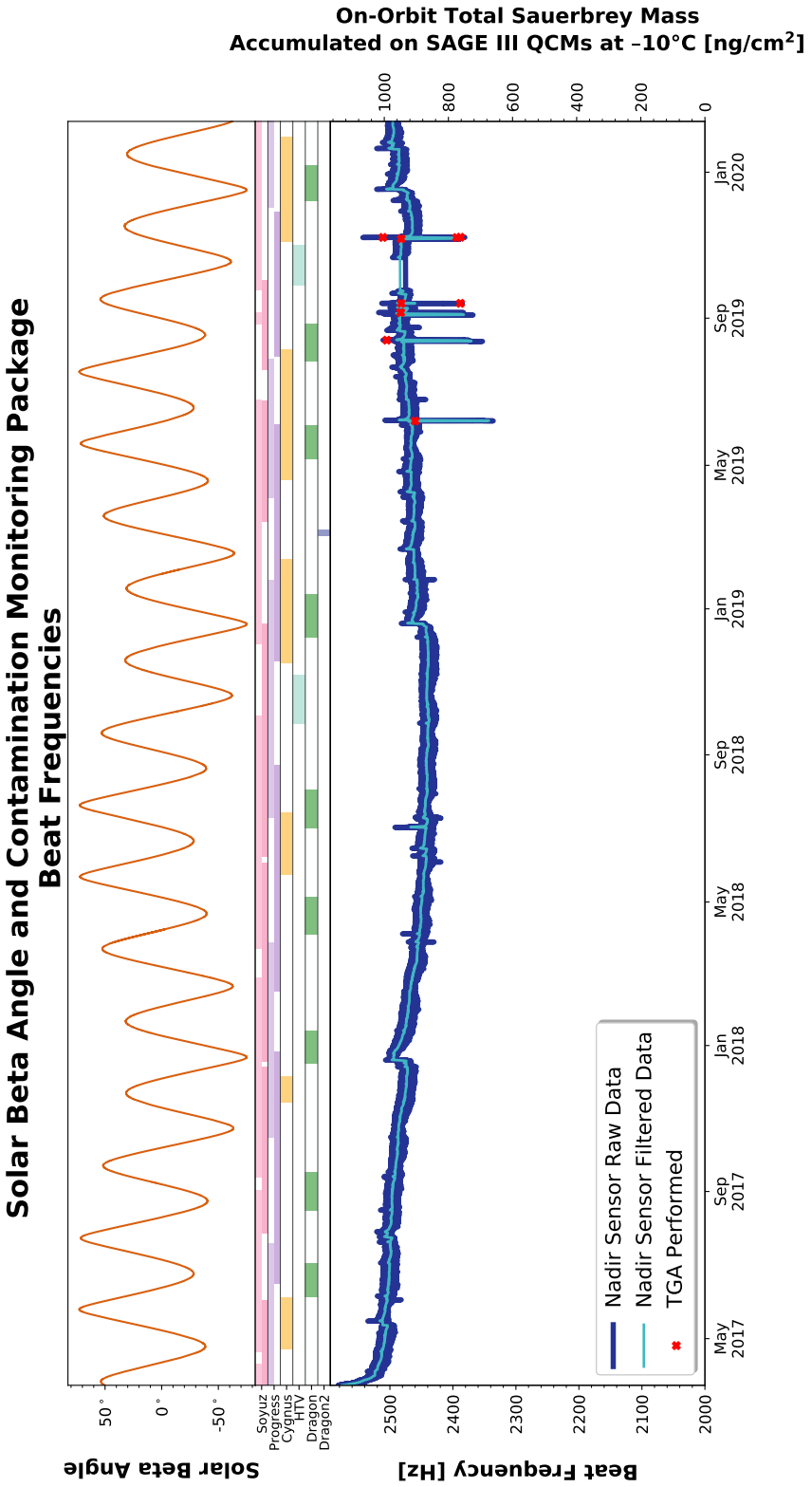

Figure B26: Timeline of Vehicles Visiting the ISS, as Seen by the Nadir Sensor

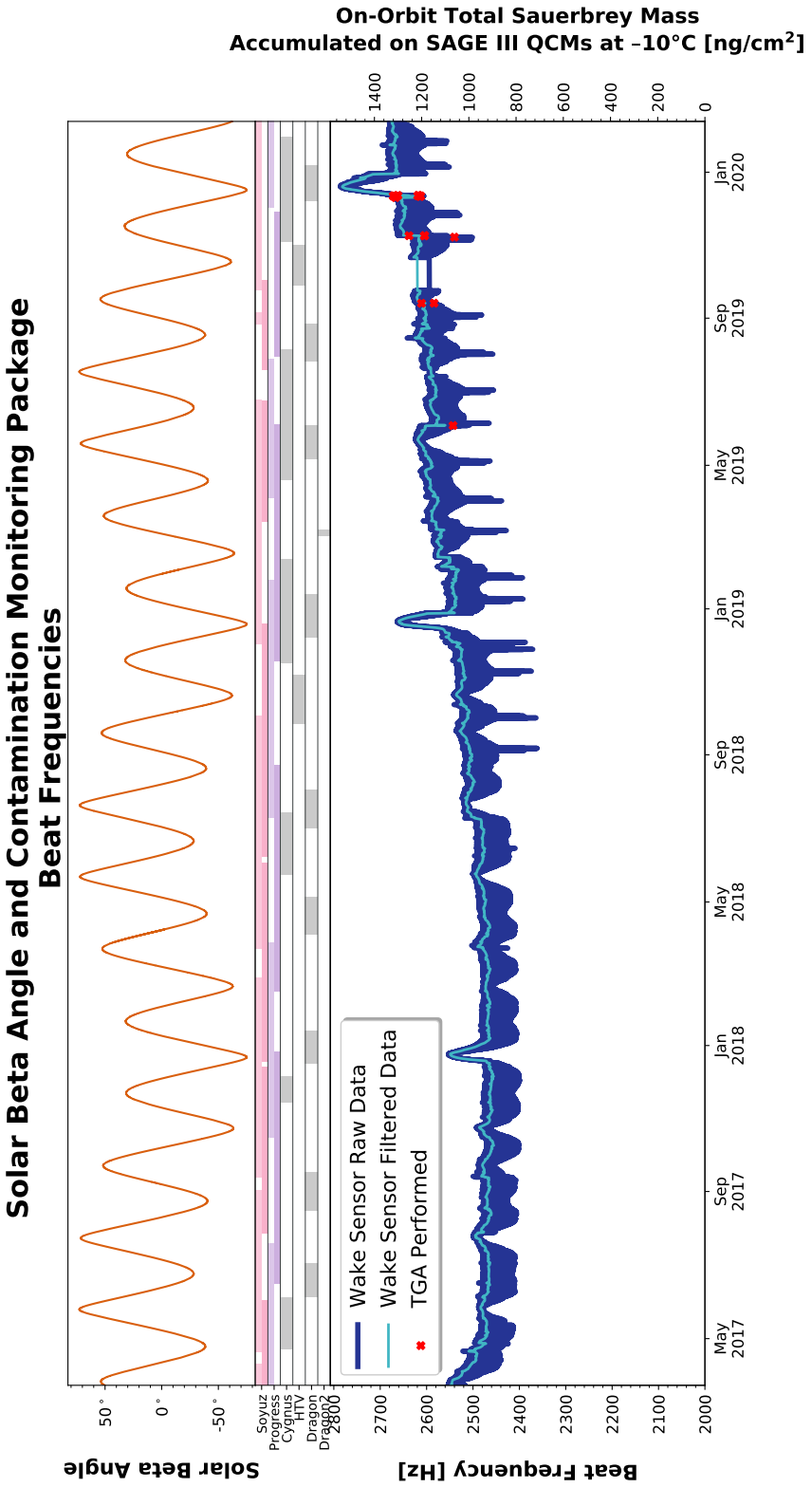

Figure B27: Timeline of Vehicles Visiting the ISS, as Seen by the Wake Sensor

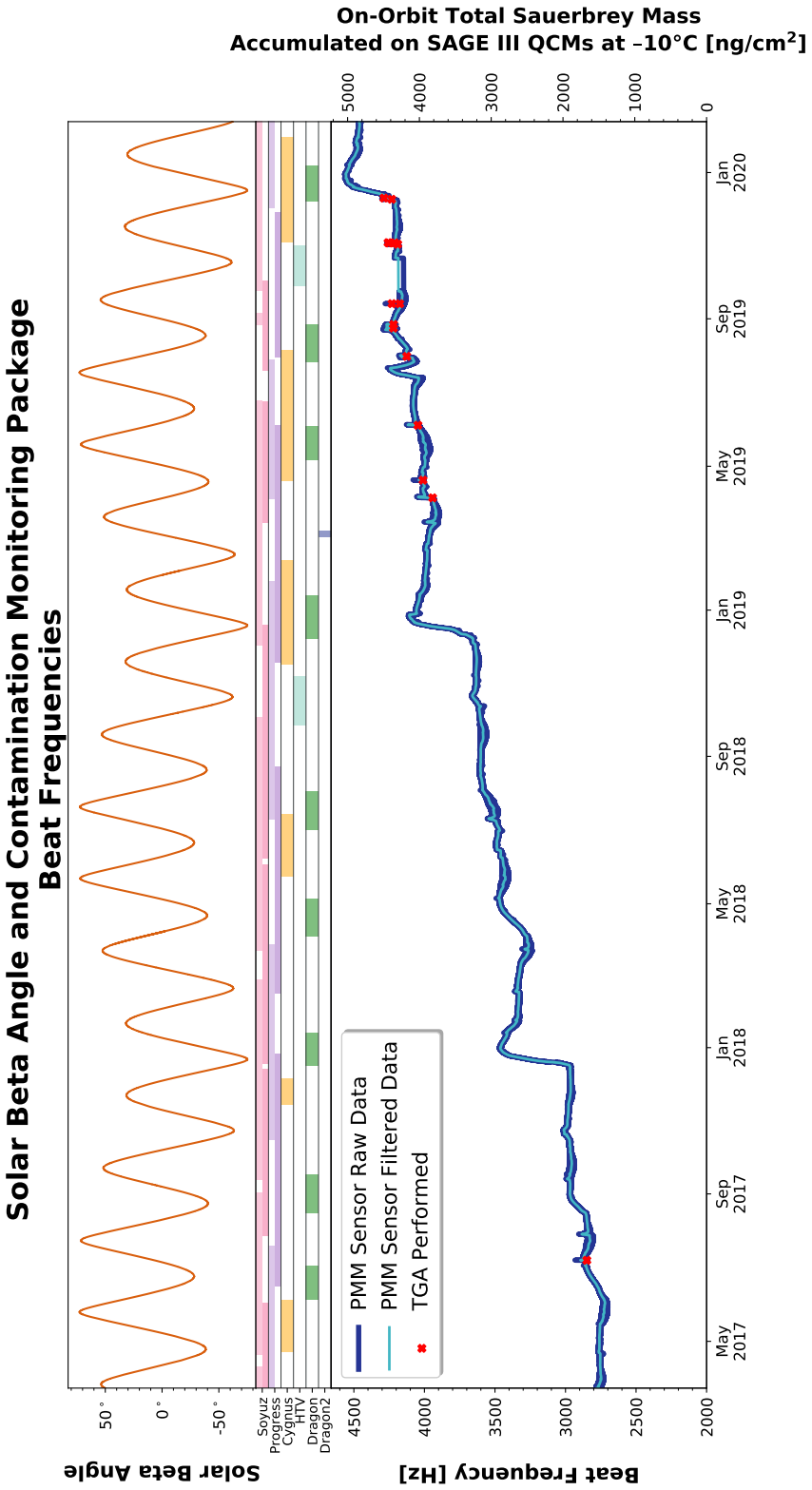

Figure B28: Timeline of Vehicles Visiting the ISS, as Seen by the PMM Sensor

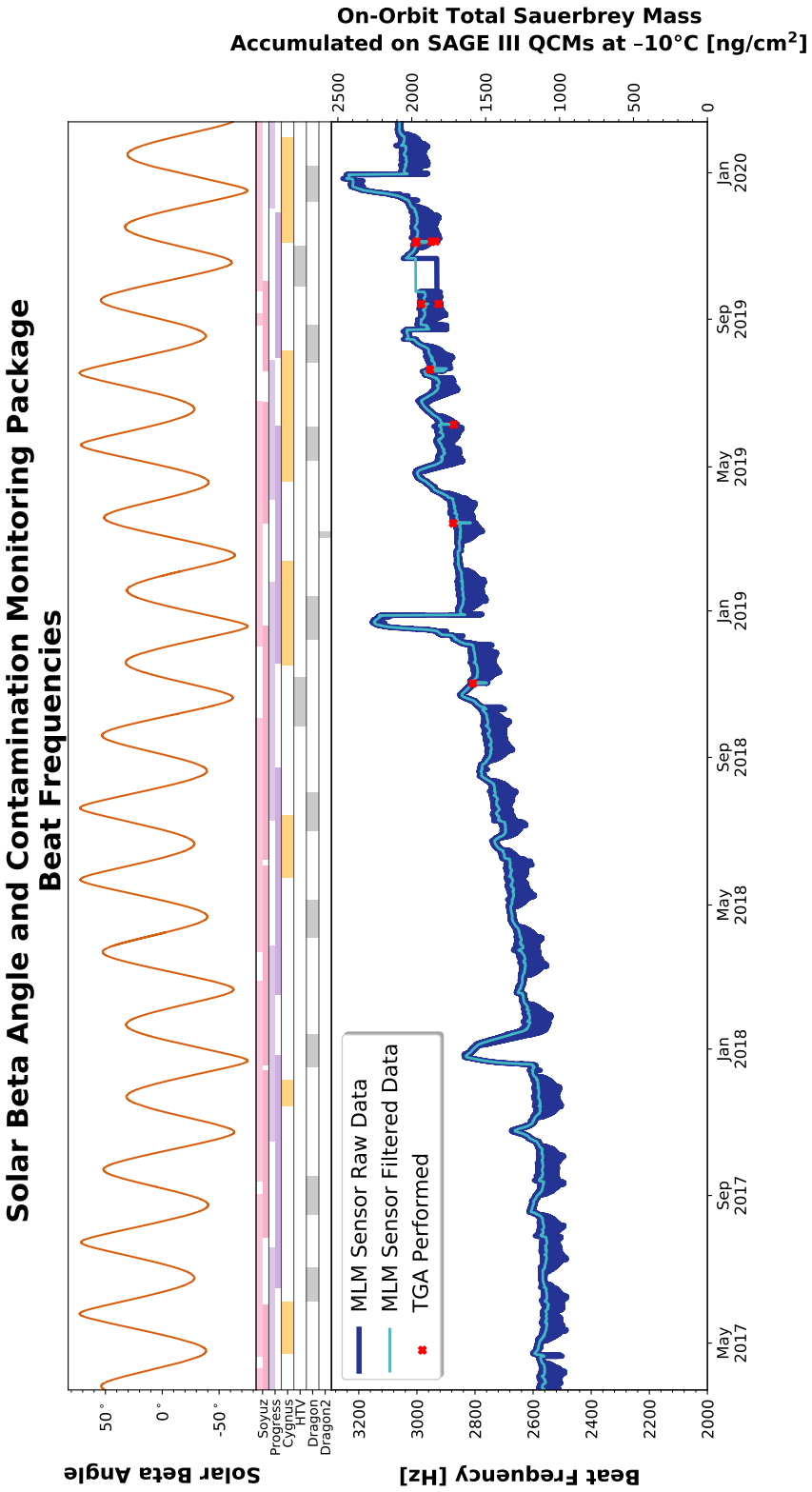

Figure B29: Timeline of Vehicles Visiting the ISS, as Seen by the MLM Sensor

Appendix C

Acronyms

AgFEP Silver-Backed Fluorinated Ethylene Propylene Teflon

AO Atomic Oxygen

BvD Butterworth-van Dyke

CMP Contamination Monitoring Package

CRS Commercial Resupply Services

ELC-4 ExPRESS Logistics Carrier-4

EVAs Extravehicular Activities

ExPA ExPRESS Payload Adapter

ExPRESS Expedite the Processing of Experiments to the Space Station

FDIR Fault Detection, Isolation, and Recovery

FOV Field of View

FPGA Field-Programmable Gate Array

HTV H-II Transfer Vehicle

IAM Interface Adapter Module

ISS International Space Station

ISSP International Space Station Program

LDEF Long Duration Exposure Facility

LEO Low Earth Orbit

MK24 TQCM Mark 24 Thermoelectric Quartz Crystal Microbalance

PCA Principal Component Analysis

PDU Power Distribution Unit

PI Proportional-Integral

PID Proportional-Integral-Differential

PRT Platinum Resistance Thermometer

QCM Quartz Crystal Microbalance

SAGE III Stratospheric Aerosol and Gas Experiment III

SAGE III–M3M SAGE III/Meteor–3M

TEC Thermoelectric Cooler

TGA Thermogravimetric Analysis

TQCM Thermoelectric Quartz Crystal Microbalance

TSM Thickness Shear Mode

UV Ultraviolet

REPORT DOCUMENTATION PAGE

Form Approved
OMB No. 0704-0188

1. REPORT DATE *(DD-MM-YYYY)*
1- 02- 2020

2. REPORT TYPE
Technical Memorandum

3. DATES COVERED *(From - To)*

4. TITLE AND SUBTITLE
SAGE III ISS Contamination Monitoring Package: Observations in Orbit

5a. CONTRACT NUMBER

5b. GRANT NUMBER

5c. PROGRAM ELEMENT NUMBER

6. AUTHOR(S)
Dawson, Tyler T.; Hill, Charles A.; Rowell, Amy F.; Leavor, Kevin R.; Hawley, Sophia

5d. PROJECT NUMBER

5e. TASK NUMBER

5f. WORK UNIT NUMBER
21606.CL2.WP3.D013.0A

7. PERFORMING ORGANIZATION NAME(S) AND ADDRESS(ES)
NASA Langley Research Center
Hampton, VA 23681-2199

8. PERFORMING ORGANIZATION REPORT NUMBER
L-21120

9. SPONSORING/MONITORING AGENCY NAME(S) AND ADDRESS(ES)
National Aeronautics and Space Administration
Washington, DC 20546-0001

10. SPONSOR/MONITOR'S ACRONYM(S)
NASA

11. SPONSOR/MONITOR'S REPORT NUMBER(S)
NASA-TM-2020-220563

12. DISTRIBUTION/AVAILABILITY STATEMENT
Unclassified - Unlimited
Subject Category 23
Availability: NASA STI Program (757) 864-9658

13. SUPPLEMENTARY NOTES

14. ABSTRACT
The Stratospheric Aerosol and Gas Experiment III (SAGE III) telescope and instrument assembly employ the methods of solar occultation and lunar occultation to retrieve near-global vertical profiles of atmospheric ozone, water vapor, nitrogen dioxide, aerosol extinctions, and other gaseous species and atmospheric state parameters. The SAGE III grating spectrometer measures light within the spectral range of 280 nm to 1037 nm at approximately 1 nm resolution, but retrievals in the Ultraviolet (UV) are particularly sensitive to contamination of the optical train. Therefore, a contamination door that contains a quartz optical window can be closed over the telescope aperture during periods of enhanced external contaminant flux. This optically transparent window permits continued science event acquisition at an acceptably diminished signal-to-noise ratio, which is expected to decline with ongoing accretion of contaminant material. To date, this impact has been short term, and science quality through the window returns to baseline performance after a contamination source is removed and spontaneous desorption removes material from the low-afinity quartz surface.

15. SUBJECT TERMS
Contamination Monitoring Package; International Space Station; Long Duration Exposure Facility; Low Earth Orbit; Outgassing; QCM Research; Quartz Crystal Microbalance; Stratospheric Aerosol and Gas Experiment; Thermogravimetric Analysis; Visiting Vehicles

16. SECURITY CLASSIFICATION OF:			17. LIMITATION OF ABSTRACT	18. NUMBER OF PAGES	19a. NAME OF RESPONSIBLE PERSON
a. REPORT	b. ABSTRACT	c. THIS PAGE			STI Help Desk (email: help@sti.nasa.gov)
U	U	U	UU	49	19b. TELEPHONE NUMBER *(Include area code)* (757) 864-9658